Using CESM-RESFire to Understand Climate-Fire-Ecosystem Interactions and the Implications for Decadal Climate Variability

Yufei Zou[1†], Yuhang Wang[1], Yun Qian[2], Hanqin Tian[3], Jia Yang[4], Ernesto Alvarado[5]

[1]School of Earth and Atmospheric Sciences, Georgia Institute of Technology, Atlanta, GA 30332, USA.
[2]Atmospheric Sciences and Global Change Division, Pacific Northwest National Laboratory, Richland, WA 99354, USA.
[3]International Centre for Climate and Global Change Research, School of Forestry and Wildlife Sciences, Auburn University, AL 36849, USA.
[4]College of Forest Resources/Forest and Wildlife Research Center, Mississippi State University, MS 39762, USA.
[5]School of Environmental and Forest Sciences, University of Washington, Seattle, WA 98195, USA.
† Now at Pacific Northwest National Laboratory, Richland, WA 99354, USA.

Correspondence to: Yuhang Wang (yuhang.wang@eas.gatech.edu) and Yufei Zou (yufei.zou@pnnl.gov)

Abstract. Large wildfires exert strong disturbance to regional and global climate systems and ecosystems by perturbing radiative forcing as well as carbon and water balance between the atmosphere and land surface, while short- and long-term variations in fire weather, terrestrial ecosystems, and human activity modulate fire intensity and reshape fire regimes. The complex climate-fire-ecosystem interactions were not fully integrated in previous climate model studies, and the resulting effects on the projections of future climate change are not well understood. Here we use a fully interactive REgion-Specific ecosystem feedback Fire model (RESFire) that was developed in the Community Earth System Model (CESM) to investigate these interactions and their impacts on climate systems and fire activity. We designed two sets of decadal simulations using CESM-RESFire for present-day (2001-2010) and future (2051-2060) scenarios, respectively and conducted a series of sensitivity experiments to assess the effects of individual feedback pathways among climate, fire, and ecosystems. Our implementation of RESFire, which includes online land-atmosphere coupling of fire emissions and fire-induced land cover change (LCC), reproduces the observed Aerosol Optical Depth (AOD) from space-based Moderate Resolution Imaging Spectroradiometer (MODIS) satellite products and ground-based AErosol RObotic NETwork (AERONET) data and agrees well with carbon budget benchmarks from previous studies. We estimate the global averaged net radiative effect of both fire aerosols and fire-induced LCC at -0.59 ± 0.52 W m^{-2}, which is dominated by fire aerosol-cloud interactions (-0.82 ± 0.19 W m^{-2}), in the present-day scenario under climatological conditions of the 2000s. The fire-related net cooling effect increases by ~170% to -1.60 ± 0.27 W m^{-2} in the 2050s under the conditions of the Representative Concentration Pathway 4.5 (RCP4.5) scenario. Such considerably enhanced radiative effect is attributed to the largely increased global burned area (+19%) and fire carbon emissions (+100%) from the 2000s to the 2050s driven by climate change. The net ecosystem exchange (NEE) of carbon between the land and atmosphere components in the simulations increases by 33% accordingly, implying that biomass burning is an increasing carbon source at short-term timescales in the future. High-latitude regions with prevalent peatlands would be more vulnerable to increased fire threats due to climate change and the increase of fire aerosols could counter the projected decrease of anthropogenic aerosols due to air pollution control policies in many

37 regions. We also evaluate two distinct feedback mechanisms that are associated with fire aerosols and fire-induced

38 LCC, respectively. On a global scale, the first mechanism imposes positive feedbacks to fire activity through enhanced

39 droughts with suppressed precipitation by fire aerosol-cloud interactions, while the second one manifests as negative

40 feedbacks due to reduced fuel loads by fire consumption and post-fire tree mortality and recovery processes. These

41 two feedback pathways with opposite effects compete at regional to global scales and increase the complexity of

42 climate-fire-ecosystem interactions and their climatic impacts.

43 **1 Introduction**

44 Large wildfires show profound impacts on human society and the environment with increasing trends in many regions

45 around the world during recent decades (Abatzoglou and Williams, 2016;Barbero et al., 2015;Clarke et al.,

46 2013;Dennison et al., 2014;Jolly et al., 2015;Westerling et al., 2006;Yang et al., 2011;Yang et al., 2015). They pose a

47 great threat to the safety of communities in the vicinity of fire-prone regions and distant downstream areas by both

48 destructive burning and increased health risks from fire smoke exposure. The global annual averaged premature deaths

49 due to fire smoke exposure was estimated about 339,000 (interquartile range: 260,000-600,000) during 1997 to 2006

50 (Johnston et al., 2012), while the total cost of fire-related socioeconomic burden would surge much higher if other

51 societal and environmental outcomes, such as morbidity of respiratory and cardiovascular diseases, expenditures of

52 defensive actions and disutility, and ecosystem service damages, were taken into account (Fann et al., 2018;Hall,

53 2014;Richardson et al., 2012;Thomas et al., 2017). In addition to hazardous impacts on human society, fire also exerts

54 strong disturbance to regional and global climate systems and ecosystems by perturbing radiation budget and carbon

55 balance between the atmosphere and land surface. In return, these short-term and long-term changes in fire weather,

56 terrestrial ecosystems, and human activity modulate fire intensity and reshape fire regimes in many climate change

57 sensitive regions. These processes were not fully included in previous climate model studies, increasing uncertainties

58 in the projections of future climate variability and fire activity (Flannigan et al., 2009;Hantson et al., 2016;Harris et

59 al., 2016;Liu et al., 2018). Most fire-related climate studies used a one-way perturbation approach by examining a

60 unidirectional forcing and response between climate change and fire activity without feedback. For instance, many

61 historical and future-projected fire responses to climate drivers were mainly based on offline statistical regression or

62 one-way coupled prognostic fire models in earth system models, while fire feedback to weather, climate, and

63 vegetation was neglected (e.g., Abatzoglou et al., 2019;Flannigan et al., 2013;Hurteau et al., 2014;Liu et al.,

64 2010;Moritz et al., 2012;Parks et al., 2016;Wotton et al., 2017;Young et al., 2017;Yue et al., 2013). The neglected

65 feedback could affect regional to global radiative forcing, biogeochemical and hydrological cycles, and ecological

66 functioning that may in turn modulate fire activity in local and remote regions (Harris et al., 2016;Liu, 2018;Pellegrini

67 et al., 2018;Seidl et al., 2017;Shuman et al., 2017). Similarly, climate studies (e.g., Jiang et al., 2016;Tosca et al.,

68 2013;Ward et al., 2012) that focused on climate responses to fire forcing used the same unidirectional approach but

69 from an opposite perspective, in which they evaluated multiple fire impacts on climate systems through fire aerosols,

70 greenhouse gases, and land albedo effects using climate sensitivity experiments with and without prescribed fire

71 emissions as model inputs. However, possible fire activity and emission changes in response to these fire weather and

72 climate variations were missing in such one-way perturbation modeling approaches.

73 To tackle these problems, we developed a two-way coupled RESFire model (Zou et al., 2019) with online land-
74 atmosphere coupling of fire-related mass and energy fluxes as well as fire-induced land cover change in CESM
75 (hereafter as CESM-RESFire). CESM-RESFire performs well using either offline observation-/reanalysis-based
76 atmosphere data or online simulated atmosphere, which is applied in this study to investigate the complex climate-
77 fire-ecosystem interactions as well as to project future climate change with fully interactive fire disturbance. In this
78 work, we use the state-of-the-science CESM-RESFire model to evaluate major climate-fire-ecosystem interactions
79 through biogeochemical, biogeophysical, and hydrological pathways and to assess future changes of decadal climate
80 variability and fire activity with consideration of these interactive feedback processes. We provide a brief model
81 description and sensitivity experiment settings in Section 2 and present modeling results and analyses on radiative
82 effects, carbon balance, and feedback evaluation in Section 3. Final conclusions and implications are followed in
83 Section 4.

2 CESM-RESFire description, simulation setup, and benchmark data

2.1 Fire model and sensitivity simulation experiments

86 RESFire (Zou et al., 2019) is a process-based fire model developed in the CESM version 1.2 modeling framework
87 that incorporates ecoregion-specific natural and anthropogenic constraints on fire occurrence, fire spread, and fire
88 impacts in both the CESM land component—the Community Land Model version 4.5 (CLM4.5) (Oleson et al., 2013)
89 and the atmosphere component—the Community Atmosphere Model version 5.3 (CAM5) (Neale et al., 2013). It is
90 compatible with either observation/reanalysis-based data atmosphere or the CAM5 atmosphere model with online
91 land-atmosphere coupling through aerosol-climate effects and fire-vegetation interactions. It includes two major fire
92 feedback pathways: the atmosphere-centric fire feedback through fire-related mass and energy fluxes and the
93 vegetation-centric fire feedback through fire-induced land cover change. These feedback pathways correspond to two
94 key climate variables, radiative forcing and carbon balance, through which fires exert their major climatic and
95 ecological impacts. Other features in CLM4.5 and CAM5, such as the photosynthesis scheme (Sun et al., 2012), the
96 3-mode modal aerosol module (MAM3; Liu et al., 2012), and the cloud microphysics (Morrison and Gettelman, 2008;
97 Gettelman et al., 2008) and macrophysics (Park et al., 2014) schemes, allow for more comprehensive assessments of
98 climate effects of fires through the interactions with vegetation and clouds. A simple treatment of secondary organic
99 aerosols (SOA) is used in CAM5 to derive SOA formation from anthropogenic and biogenic volatile organic
100 compounds (VOCs) with fixed mass fields (Table S1 in the Supplement). The total SOA mass is emitted as the SOA
101 (gas) species from the surface and then condensation/evaporation of gas-phase SOA to/from different aerosol modes
102 are calculated in the MAM3 module (Neale et al., 2013). The gas-phase photochemistry is not included in the CAM5
103 simulations, which precludes the possibility for evaluating chemistry-climate interactions. We also implement
104 distribution mapping-based online bias corrections for key fire weather variables (i.e., surface temperature,
105 precipitation, and relative humidity) to reduce negative influences of climate model biases in atmosphere simulation
106 and projection. Fire plume rise is globally universal parameterized based on atmospheric boundary layer height
107 (PBLH), fire radiative power (FRP), and Brunt-Väisälä frequency in the free troposphere (Sofiev et al., 2012). Please
108 refer to Zou et al. (2019) for more detailed fire model descriptions and to Sofiev et al. (2012) for the fire plume rise

109   parameterization. To quantify the impacts of fire-climate interactions under different climatic conditions, we designed

110   two groups of sensitivity simulations for present-day and future scenarios (Table 1). In each simulation group, we

111   conducted one control run (CTRLx, where x=1 or 2 indicates the present-day or future scenario, respectively) and two

112   sensitivity runs (SENSxA/B, where x is the same as that in CTRL runs and the notations of A and B are explained

113   below). The CTRL runs were designed with fully interactive fire disturbance such as fire emissions with plume rise

114   and fire-induced LCC with different boundary conditions for a present-day scenario (CTRL1; 2001-2010) and a

115   moderate future emission scenario (CTRL2) of the Representative Concentration Pathway 4.5 (RCP4.5; 2051-2060),

116   respectively. In each scenario, we turned off the atmosphere-centric feedback mechanisms (e.g., fire aerosol climate

117   effects) in SENSxA simulations (where x=1 or 2) and then turned off both atmospheric-centric and vegetation-centric

118   fire feedback (e.g., fire-induced LCC) in SENSxB simulations. Consequently, we estimated the atmosphere-centric

119   impacts of fire emissions on radiative forcing in the present-day scenario (RCP4.5 future scenario) by comparing

120   SENS1A (SENS2A) with CTRL1 (CTRL2). We also estimated the vegetation-centric impacts of fire-induced LCC

121   on terrestrial carbon balance in the present-day scenario (RCP4.5 future scenario) by comparing SENS1B (SENS2B)

122   with SENS1A (SENS2A). The net fire-related effects were evaluated by comparing CTRL runs with SENSxB runs

123   as both fire feedback mechanisms were turned off in the SENSxB runs. Using these sensitivity experiments, we are

124   able to evaluate two-way climate-fire-ecosystem interactions under the same integrated modeling framework that is

125   not possible in one-way perturbation studies considering either climate impacts on fires (Kloster et al., 2010;Kloster

126   et al., 2012;Thonicke et al., 2010) or fire feedback to climate (Jiang et al., 2016;Li et al., 2014;Ward et al., 2012;Yue

127   et al., 2015;Yue et al., 2016).

128   **2.2 Model input data**

129   We used the spun-up files from previous long-term runs (Zou et al., 2019) as initial conditions for the present-day

130   experiments (CTRL1 and SENS1A/B). The boundary conditions including the prescribed climatological (1981-2010

131   average) sea surface temperature and sea ice data for the present-day scenario were obtained from the Met Office

132   Hadley Centre (HadISST) (Rayner et al., 2003). Similarly, the nitrogen and aerosol deposition rates were also

133   prescribed from a time-invariant spatially varying annual mean file for 2000 and a time-varying (monthly cycle)

134   globally-gridded deposition file, respectively, as the standard datasets necessary for the present-day CAM5

135   simulations (Hurrell et al., 2013). The climatological 3-hourly cloud-to-ground lightning data via bilinear interpolation

136   from NASA LIS/OTD grid product v2.2 (http://ghrc.msfc.nasa.gov) 2-hourly lightning frequency data and the world

137   population density data were fixed at the 2000 levels for all the present-day simulations. The non-fire emissions from

138   anthropogenic sources (e.g., industrial, domestic and agriculture activity sectors) in the present-day scenario were

139   from the emission dataset (Lamarque et al., 2010) representing year 2000 for the Fifth Assessment Report of the

140   Intergovernmental Panel on Climate Change (IPCC AR5). Emissions of natural aerosols such as dust and sea salt were

141   calculated online (Neale et al., 2013), while vertically resolved volcanic sulfur and dimethyl sulfide (DMS) emissions

142   were prescribed from the AEROCOM emission dataset (Dentener et al., 2006). Emission fluxes for the 5 VOC species

143   (isoprene, monoterpenes, toluene, big alkenes, and big alkanes) to derive SOA mass yields were prescribed from the

144   MOZART-2 dataset (Horowitz et al., 2003). For fire emissions, we replaced the prescribed GFED2 fire emissions

145 (van der Werf et al., 2006) from the default offline emission data with online coupled fire emissions generated by the

146 RESFire model in the CTRL runs. We then decoupled online simulated fire emissions in the SENS1A runs, in which

147 fire emissions were not transported to the CAM5 atmosphere model, to isolate the atmosphere-centric impacts of fire-

148 climate interactions. In both CTRL1 and SENS1A experiments, we allowed the semi-static historical LCC data for

149 the year 2000 from the version 1 of the Land-Use History A product (LUHa.v1) (Hurtt et al., 2006) to be affected by

150 post-fire vegetation changes (Zou et al., 2019). We then used the fixed LCC data for the year 2000 in the SENS1B

151 run and compared two SENS1 runs (SENS1A-SENS1B) to evaluate the vegetation-centric fire impacts on terrestrial

152 ecosystems and carbon balance in the 2000s.

153 For the future scenario experiments, we replaced all the present-day datasets with the RCP4.5 projection datasets

154 including the initial conditions and prescribed boundary conditions of global SST and sea ice data in 2050, the cyclical

155 non-fire emissions and deposition rates fixed in 2050 under the RCP4.5 scenario, and the annual LCC data for the

156 RCP4.5 transient period in 2050 based on the Future Land-Use Harmonization A products (LUHa.v1_future) (Hurtt

157 et al., 2006). All these datasets were described in the technical note of CAM5 (Neale et al., 2013) and stored on the

158 Cheyenne computing system (CISL, 2017) at the National Center for Atmospheric Research (NCAR)-Wyoming

159 Supercomputing Center (NWSC). It is worth noting that we used the present-day demographic data and observation-

160 based climatological lightning data in the future scenario given pathway-dependence and great uncertainties in future

161 projections of these inputs (Clark et al., 2017;Riahi et al., 2017;Tost et al., 2007;). In other words, we did not consider

162 the influence of fire ignition changes associated with human activity or lightning flash density in our future projection

163 simulations but focused on broad impacts of future climate change on fuel loads and combustibility as well as fire

164 weather conditions.

165 The global mean greenhouse gas (GHG) mixing ratios in the CAM5 atmosphere model were fixed at the 2000-year

166 levels (CO_2: 367.0 ppmv; CH_4:1760.0 ppbv; N_2O:316.0 ppbv) in all present-day experiments and they were replaced

167 by the prescribed RCP4.5 projection datasets with the well-mixed assumption and monthly variations in the future

168 scenarios. These GHG mixing ratios were then passed to the CLM4.5 land model in all sensitivity experiments. In

169 return, the land model provided the diagnostics of the balance of all carbon fluxes between net ecosystem production

170 (NEP, g C m^{-2} s^{-1}, positive for carbon sink) and depletion from fire emissions, landcover change fluxes, and carbon

171 loss from wood products pools, and then the computed net CO_2 flux was passed to the atmosphere model in forms of

172 net ecosystem exchange (NEE, g C m^{-2} s^{-1}). Though fire emissions could perturb the value of NEE at short-term scales,

173 it is often assumed that fire is neither a source nor a sink for CO_2 since fire carbon emissions are offset by carbon

174 absorption of vegetation regrowth over long-term scales (Bowman et al., 2009). Therefore, we did not consider the

175 radiative effect of fire-related GHGs in our sensitivity experiments. This kind of "concentration-driven" simulations

176 with prescribed atmospheric CO_2 concentrations for a given scenario have been used extensively in previous fire-

177 climate interaction assessments (e.g., Kloster et al., 2010;Li et al., 2014;Thonicke et al., 2010) and most of the RCP

178 simulations (Ciais et al., 2013).

179 **2.3 Model evaluation benchmarks and datasets**

180 Multiple observational and assimilated datasets were applied to evaluate the modeling performance regarding radiative

181 forcing. We collected space-based column aerosol optical depth (AOD) from the level-3 MODIS Aqua monthly global

182 product (MYD08_M3, Platnick et al., 2015) and ground-based version 3 aerosol optical thickness (AOT) level 2.0

183 data from the Aerosol Robotic Network (AERONET, https://aeronet.gsfc.nasa.gov/) project for comparison with the

184 model simulated AOD data at 550 nm. The AERONET AOT at 550 nm were interpolated by estimating Ångström

185 exponents based on the measurements taken at two closest wavelengths at 500 nm and 675 nm (see the Supplement

186 for details). We then followed the Ghan method (Ghan, 2013) to estimate fire aerosol radiative effects (RE_{aer}) on the

187 planetary energy balance in terms of aerosol-radiation interactions (RE_{ari}), aerosol-cloud interactions (RE_{aci}), and fire

188 aerosol-related surface albedo change (RE_{sac}) in Eq. (1). The radiative effect related to fire-induced land cover change

189 (RE_{lcc}) was estimated by comparing shortwave radiative fluxes at the top-of-atmosphere (TOA) between SENSxA

190 (with fire-induced LCC) and SENSxB (without fire-induced LCC) experiments. By summing up all these terms, we

191 estimated the fire-related net radiative effect (RE_{fire}) as the shortwave radiative flux difference between CTRLx (with

192 fire aerosols and fire-induced LCC) and SENSxB (without fire aerosols and fire-induced LCC) experiments:

$$
\begin{aligned}
&RE\ of\ interaction\ of\ radiation\ with\ fire\ aerosol\colon RE_{ari} = \Delta(F - F_{clean})\\
&RE\ of\ interaction\ of\ clouds\ with\ fire\ aerosol\colon RE_{aci} = \Delta\big(F_{clean} - F_{clear,clean}\big)\\
&RE\ of\ surface\ albedo\ change\ induced\ by\ fire\ aerosol\colon RE_{sac} = \Delta F_{clear,clean}\\
&net\ RE\ of\ fire\ aerosol\colon RE_{aer} = RE_{ari} + RE_{aci} + RE_{sac} = F_{CTRLx} - F_{SENSxA}\\
&RE\ of\ fire\ induced\ land\ cover\ change\colon RE_{lcc} = F_{SENSxA} - F_{SENSxB}\\
&net\ RE\ of\ fire\colon RE_{fire} = RE_{aer} + RE_{lcc} = F_{CTRLx} - F_{SENSxB}
\end{aligned}
\tag{1}
$$

193

194 where Δ is the difference between control and sensitivity simulations, F is the shortwave radiative flux at the TOA,

195 F_{clean} is the radiative flux calculated as an additional diagnostics from the same simulations but neglecting the

196 scattering and absorption of solar radiation by all aerosols, and $F_{clear,clean}$ is the flux calculated as additional

197 diagnostic but neglecting scattering and absorption by both clouds and aerosols. The surface albedo effect is largely

198 the contribution of changes in surface albedo induced by fire aerosol deposition and land cover change, which is small

199 but non-negligible in some regions (Ghan, 2013). We used similar modeling settings including the 3-mode modal

200 aerosol scheme (MAM3) (Liu et al., 2012) and the Snow, Ice, and Aerosol Radiative (SNICAR) module (Flanner and

201 Zender, 2005) and compared our online coupled fire modeling results against previous offline prescribed fire modeling

202 studies (Jiang et al., 2016; Ward et al., 2012) in the next section.

203 We also examined the modeling performance on burned area and terrestrial carbon balance such as fire carbon

204 emissions, gross primary production (GPP, g C m^{-2} s^{-1}, positive for vegetation carbon uptake), net primary production

205 (NPP, g C m^{-2} s^{-1}, positive for vegetation carbon uptake), net ecosystem productivity (NEP, g C m^{-2} s^{-1}, positive for

206 net ecosystem carbon uptake), and net ecosystem exchange (NEE, g C m^{-2} s^{-1}, positive for net ecosystem carbon

207 emission). The model simulated burned area and fire carbon emissions were evaluated against the satellite based

208 GFED4.1s datasets (Giglio et al., 2013; Randerson et al., 2012; van der Werf et al., 2017), and these carbon budget

209 related variables were calculated in Eqs. (2) and (3) and compared with the MODIS primary production products

210 (Zhao et al., 2005; Zhao and Running, 2010), previous modeling results used for terrestrial model comparison projects

211 (Piao et al., 2013) and the IPCC AR5 report (Ciais et al., 2013), and the global carbon budget assessment (Le Quere

212 et al., 2013) by the broad carbon cycle science community.

213 $\quad$ GPP = NPP + R_a = (NEP + R_h) + R_a, $\hspace{6cm}$ (2)

214 $\quad$ NEE = C_{fe} + C_{lh} − NEP = C_{fe} + C_{lh} + R_h + R_a − GPP, $\hspace{4cm}$ (3)

215 where R_a is the total ecosystem autotrophic respiration (g C m^{-2} s^{-1}), R_h is the total heterotrophic respiration (g C m^{-2}

216 s^{-1}), C_{fe} is the fire carbon emissions (g C m^{-2} s^{-1}), and C_{lh} is the carbon loss (g C m^{-2} s^{-1}) due to land cover change,

217 wood products, and harvest.

218 **3 Modeling results and discussion**

219 **3.1 Evaluation of fire-related radiative effects**

220 Figure 1 shows the comparison of the model simulated 10-year annual averaged column AOD at 550nm from CTRL1

221 and space-based AOD from MODIS aboard the Aqua satellite. It's noted that both AOD data result from all sources

222 including fire and non-fire emissions, and significant differences exist in specific regions due to large biases in model

223 emission inputs and aerosol parameterization. In the MODIS AOD data, the most noticeable hotspot regions include

224 eastern China, South Asia such as India, and Africa. The first two regions are contributed mostly by anthropogenic

225 emissions, while the last one is dominated by fire emissions. Since the non-fire emissions used in CAM5 simulations

226 are 2000-based (Lamarque et al., 2010) and low biased comparing to rapid emission increases in many Asian

227 developing countries (Kurokawa et al., 2013), the simulated hotspot regions in East and South Asia are not as

228 appreciable as those observed in the remote sensing data. The model results also show underestimation in rainforests

229 over South America and Central Africa, where large fractions of aerosols are contributed by primary and secondary

230 organic aerosols from biogenic sources and precursors (Gilardoni et al., 2011) that are missing in the simulation.

231 Another possible cause for the underestimation problem is underrepresented burning activity due to deforestation and

232 forest degradation and consequently underestimated fire aerosols emissions in these regions. The AOD simulations

233 over tropical savanna regions with pervasive biomass burning activities are also lower than the satellite observations,

234 which might be attributable to both underestimated online fire emissions and too strong wet scavenging of primary

235 carbonaceous aerosols in the CAM5-MAM3 model (Liu et al., 2012). The CAM5 model overestimates dust emissions

236 significantly with some spuriously high AOD hotspots emerging over the Sahara, Arabian, South Africa, and Central

237 Australia desert regions. This dust AOD overestimation problem was also found in a previous dust modeling study

238 using the release version of the CAM5-MAM3 model (Albani et al., 2014).

239 $\quad$ To further evaluate the fire-related AOD modeling performance, we compare the difference between CTRL1 and

240 SENS1A to isolate aerosol contributions from fire sources in Fig. 2. The spatial distribution of fire-related AOD

241 clearly highlighted African savanna as a major biomass burning region. We also compare monthly AOD at six fire-

242 prone regions with AERONET observations to get a better understanding of temporal variations of fire aerosols. Most

243 sites show strong seasonal variations in monthly AOD as observed by AERONET, and the CESM-RESFire model

244 well capture fire seasonality in these regions. Generally, the model AOD results are at the lower ends of the uncertainty

245 ranges of ground-based observations in most regions due to limited spatial representativeness of coarse model grid

246   resolution and fire emissions, especially over African savannas like Ilorin (Fig. 2e) and Southeast Asian rainforests
247   like Jambi (Fig. 2g) where agricultural and deforestation related burning activity prevails.

248   Lastly, we estimate present-day radiative effects of fire aerosols and fire-induced land cover change and compare
249   the results with previous studies in Fig. 3 and Table 2. The radiative effect of fire aerosol-radiation interactions (RE_{ari})
250   is most prominent in tropical Africa and downwind Atlantic Ocean areas as well as South America and eastern Pacific.
251   High-latitude regions like eastern Siberia also show significant positive radiative effects due to fire emitted light
252   absorbing aerosols such as black carbon (BC). The land-sea contrast of radiative warming and cooling effects over
253   Africa and South America are attributed to differences of cloud cover fractions over land and ocean areas (Jiang et al.,
254   2016). In these regions, cloud fractions and liquid water path are much larger over downwind ocean areas than land
255   areas during the fire season. Cloud reflection of solar radiation strongly enhances light absorption by fire aerosols
256   residing above low-level marine clouds (Abel et al., 2005; Zhang et al., 2016).

257   The radiative effect of fire aerosol-cloud interactions (RE_{aci}) shows generally cooling effects in most regions due to
258   scattering and reflections by enhanced cloudiness, and these cooling effects are more pervasive over high-latitude
259   regions such as boreal forests in North America and eastern Siberia. The land-sea contrast of radiative effects emerges
260   again in the vicinity of Africa and South America, but the signs of the contrasting effect related with aerosol-cloud
261   interactions are opposite to these from aerosol-radiation interactions. The large amounts of fire aerosols suppress low-
262   level clouds over the African land region by stabilizing the lower atmosphere through reduction of radiative heating
263   of the surface. However, fire aerosols increase cloud cover and brightness in the downwind Atlantic Ocean areas
264   because they increase the number of cloud condensation nuclei and the larger cloud droplet number density reduce
265   cloud droplet sizes (Lu et al., 2018; Rosenfeld et al., 2019; Fig. S1 in the Supplement). The radiative effect of fire
266   aerosol-related surface albedo change (RE_{sac}) shows contrasting radiation effects with strong warming effects over
267   most Arctic regions caused by deposition of light-absorbing aerosol over ice and snow and reduction of surface albedo,
268   but moderate cooling effects in boreal land regions such as Canada and eastern Siberia, which are related to fire
269   aerosol-induced snowfall and snow cover change and associated surface albedo change (Ghan, 2013; Fig. S2 in the
270   Supplement). Besides spatial heterogeneity in fire-induced radiative effects, these radiative effects also show
271   significant temporal variations that are related with fire seasonality. Figure 4 shows zonal averaged time-latitude cross
272   sections of fire aerosol emissions and fire-induced changes in clouds and radiative effects. Massive fire carbonaceous
273   emissions shift from the Northern Hemisphere tropical regions in boreal winter to the Southern Hemisphere tropical
274   regions in boreal summer, when similar amounts of fire emissions are also observed in boreal mid- and high-latitude
275   regions (Fig. 4a/b). Fire aerosols greatly increase cloud condensation nuclei (CCN, Fig. 4c) and cloud droplet number
276   concentrations (CDNUMC, Fig. 4d) in these regions, while the increase in cloud water path (CWP, Fig. 4e) and low
277   cloud fraction (CLDLOW, Fig. 4f) are more significant in boreal high-latitude regions than in the tropics. The low
278   solar zenith angle in high-latitude regions enhances solar radiation absorption by light-absorbing aerosols and results
279   in stronger changes in radiative effects by aerosol-radiation interactions during boreal summer (Fig. 4g). In the
280   meantime, increased CWP and CLDLOW in high-latitude regions also lead to much stronger cooling effects by
281   aerosol-cloud interactions (RE_{aci}) (Fig. 4h), which overwhelm the increase in RE_{ari}. These modeling results based on
282   the online coupled RESFire model show similar spatiotemporal patterns with these in Jiang et al. (2016), which used

283   the same version of the CAM5 atmosphere model with a 4-mode modal aerosol module (MAM4) that was driven by

284   offline prescribed fire emissions.

285   In general, the 10-year averaged global mean values and standard deviations of interannual variations for fire

286   aerosol-related RE_{ari}, RE_{aci}, and RE_{sac} in the 2000s are -0.003 ± 0.013 W m^{-2}, -0.82 ± 0.19 W m^{-2}, and 0.19 ± 0.61 W

287   m^{-2}, respectively, and fire-induced RE_{lcc} is 0.04 ± 0.38 W m^{-2}. After combining all these forcing terms, we estimate a

288   net RE_{fire} of -0.59 ± 0.51 W m^{-2} for the present-day scenario that is larger than the estimate of -0.55 W m^{-2} in the

289   previous fire radiative effect studies (Jiang et al., 2016;Ward et al., 2012). It is noted that both Ward et al. (2012) and

290   Jiang et al. (2016) used prescribed fire emissions from CLM3 model simulations (Kloster et al., 2010;Kloster et al.,

291   2012) and GFED datasets (Giglio et al., 2013;Randerson et al., 2012), respectively, for their uncoupled fire sensitivity

292   simulations. The annual fire carbon emissions used by Ward et al. (2012) ranged from 1.3 Pg C yr^{-1} for the present-

293   day simulation to 2.4 Pg C yr^{-1} for the future projection with ECHAM atmospheric forcing, while the fire BC, POM

294   and SO$_2$ emissions used by Jiang et al. (2016) were based on the GFEDv3.1 dataset with an annual averaged fire

295   carbon emission of 1.98 Pg C yr^{-1} (Randerson et al., 2012). Their fire emissions are lower than the RESFire model

296   simulation of 2.6 Pg C yr^{-1} (Table 3) in this study, which contribute to the differences in the estimates of fire aerosol

297   radiative effects. It is also worth noting that all fire emissions were released into the lowest CAM level as surface

298   sources by Ward et al. (2012), and a default vertical profile of fire emissions based on the AEROCOM protocol

299   (Dentener et al., 2006) was used by Jiang et al. (2016) in their CAM5 simulations. In our simulations, we used a

300   simplified plume rise parameterization (Sofiev et al., 2012) based on online calculated fire burning intensity (FRP)

301   and atmospheric stability conditions (PBLH and Brunt-Väisälä frequency) in CESM-RESFire and applied vertical

302   profiles with diurnal cycles to the vertical distribution of fire emissions. The simulations of annual median heights of

303   fire plumes for the present-day and RCP4.5 future scenarios are shown in Fig. 5. Previous observation-based injection

304   height studies suggested that only 4–12% fire plumes could penetrate planetary boundary layers with most fire plumes

305   stay within the near surface atmosphere layers (val Martin et al., 2010). Our plume-rise simulation results agree with

306   these estimates, though a quantitative comparison is beyond the scope of this study because of the inconsistency

307   between simulated and actual meteorological conditions. It is also noted that there is no systematic change in plume

308   rise height distributions between the RCP4.5 future scenario and present-day scenarios, both of which show most fire

309   plumes (~80%) rise less than 1000 m. Comparing to surface released fire emissions in previous studies (Ward et al.,

310   2012), our higher elevated fire plumes affect the vertical distribution and lifetime of fire aerosols and further influence

311   regional radiative effects after long-range transport of fire aerosols.

312   **3.2 Fire-related disturbance to carbon balance**

313   In addition to the atmosphere-centric fire-induced radiative effects, we also quantify the vegetation-centric terrestrial

314   carbon budget changes to evaluate fire disturbance to terrestrial ecosystems. We use the previous model inter-

315   comparison studies and the latest GFEDv4.1s datasets as evaluation benchmarks and examine fire-related metrics

316   including global burned area and fire carbon emissions (Fig. 6 and Table 3). We also collect global scale GPP, NPP,

317   and NEE from previous literatures (Ciais et al., 2013; Piao et al., 2013;Zhao and Running, 2010) to compare with our

318   simulation results (Table 3). The RESFire model performs well in global burned area and fire carbon emissions driven

by either offline observation-/reanalysis-based CRUNCEP atmosphere data (RESFire_CRUNCEP) and online CAM5 simulated atmosphere data after bias corrections (RESFire_CAM5c). The annual averaged burned area results of both RESFire_CRUNCEP (508 ± 15 Mha yr^{-1}) and RESFire_CAM5c (472 ± 14 Mha yr^{-1}) are very close to the GFEDv4.1s benchmark value of 510 ± 27 Mha yr^{-1}, while the default fire model in CLM (322 Mha yr^{-1}) is significantly low biased. For fire carbon emissions, the offline RESFire_CRUNCEP result (2.3 ± 0.2 Pg C yr^{-1}) agrees well with the GFEDv4.1s benchmark of around 2.2 ± 0.4 Pg C yr^{-1}, and the online RESFire_CAM5c result shows a 18% higher value (2.6 ± 0.1 Pg C yr^{-1}) than the benchmark. Since the GFED emission datasets are low biased due to low satellite detection rates for small fires under canopy and clouds, previous fire studies (Johnston et al., 2012;Ward et al., 2012) rescaled fire emissions in their practice for climate and health impact assessment. Here, a moderate increase in online estimated fire carbon emissions would reduce the need for fire emission rescaling. Such difference is also consistent with the changes in different versions of the GFED datasets, which show a 11% increase of global fire carbon emissions in the latest GFED4s as compared with the old GFED3 for the overlapping 1997-2011 time period (van der Werf et al., 2017). This increased global fire carbon emissions in the GFED4s dataset result from a substantial increase in global burned area (+37%) due to inclusion of small fires and a modest decrease in mean fuel consumption (-19%) according to van der Werf et al. (2017). Since carbon emissions from deforestation fires and other land use change processes are a key component to estimate global carbon budget (Le Quere et al., 2013), improved fire emission estimation would benefit carbon budget simulation in the land model.

We then compare the CLM simulated carbon budget variables such as GPP and NEE against 10 process-based terrestrial biosphere models that were used for the IPCC fifth Assessment Report (Piao et al., 2013). Both the offline and online CLM GPP results are around 142 Pg C yr^{-1}, which are higher than the MODIS primary production products (MOD17) of 109.29 Pg C yr^{-1} (Zhao et al., 2005) and near the upper bound of ensemble modeling results (133 ± 15 Pg C yr^{-1}) (Piao et al., 2013). Such high GPP estimation leads to ~11% higher NPP in the CLM simulations than the MODIS global average annual NPP product of 53.5 Pg C yr^{-1} from 2001 to 2009 (Zhao and Running, 2010) as well as the old modeling result (54 Pg C yr^{-1}) based on the default fire model in CLM developed by Li et al. (2013;2014) (hereafter as CLM-LL2013). These differences may result from the different atmosphere forcing data used to drive the CLM land model. However, the NEE results based on the CESM-RESFire model are consistent with the benchmarks from the IPCC AR5 (Ciais et al., 2013) and ensemble modeling results (Piao et al., 2013), indicating a good land modeling performance with online fire disturbance in CESM.

After the evaluation of carbon budget in the CLM land model, we further decompose the components in NEE and compare the new CESM-RESFire simulation results with previous fire model simulations by Li et al. (2014). Following their experiment setting in Li et al. (2014), we isolate fire contributions to each carbon budget variables by differencing the fire-on and fire-off experiments driven by the CRUNCEP data atmosphere in Table 4. We find a 58% increase in fire-induced NEE variations simulated by CESM-RESFire than CLM-LL2013. This increase is attributed to enhanced fire emissions and suppressed NEP in CESM-RESFire. As discussed in the previous section, CESM-RESFire simulates higher annual averaged fire carbon emissions (2.08 Pg C yr^{-1}) than CLM-LL2013 (1.9 Pg C yr^{-1}), which contributes 31% of the difference in their NEE changes. Furthermore, CESM-RESFire simulates smaller NEP changes due to fire disturbance, which is attributable to fire-induced land cover change in RESFire. Fire-induced

whole plant mortality and post-fire vegetation recovery are implemented in the new CESM-RESFire model (Zou et al., 2019), both of which are not included in the default CLM-LL2013 model. The newly incorporated fire-induced land cover change would influence ecosystem productivity and respiration as shown by carbon budget variables in Table 4. Specifically, the fire-induced whole plant mortality and recovery would moderate the variations in ecosystem productivity and respiration and further suppress fire-induced NEP changes. The suppressed NEP change explains 52% of the total difference between CESM-RESFire and CLM-LL2013 in simulated NEE changes.

Similar suppression effects of fires on NEP were also found in Seo and Kim (2019), in which they used the CLM-LL2013 fire model but enabled the dynamic vegetation (DV) mode to simulate post-fire vegetation changes. Though the DV mode of the CLM model is capable of simulating vegetation dynamics, considerable biases exist in the online simulation of land cover change by the coupled CLM-DV model (Quillet et al., 2010) and may undermine the interpretation of fire-related ecological effects. For instance, the global fractions of bare ground and needleleaf trees in the CLM-DV simulations are much larger than these in the non-DV (BGC only) simulation in Seo and Kim (2019), while the fractions of shrub and broadleaf trees with active DV are less than these without DV regardless of whether fire disturbance are included or not in the simulations. These biases could distort ecosystem properties such as primary production and carbon exchange as well as fire-related ecological effects.

Similar to fire-related radiative effects, we examine changes of carbon budget variables in the RCP4.5 future scenario in Table 5 and Fig. 7. The global burned area increases by 19% from the present-day scenario in CTRL1 (464 $\pm$ 19 Mha yr^{-1}) to the RCP4.5 future scenario in CTRL2 (551 $\pm$ 16 Mha yr^{-1}) (Fig. 7a). Accordingly, the annual averaged fire carbon emission increases by 100% from 2.5 $\pm$ 0.1 Pg C yr^{-1} at present to 5.0 $\pm$ 0.3 Pg C yr^{-1} in the future (Fig. 7b). This increase is larger than a previous CLM simulated result of 25%~52% by Kloster et al. (2010;2012), which might result from different climate sensitivity between CESM-RESFire and the old fire model in CLM. It's noted that recent satellite-based studies found decreasing trends in burned area over specific regions such as Northern Hemisphere Africa driven by human activity and agricultural expansion (Andela and van der Werf, 2014; Andela et al., 2017). Though we mainly focus on fire-climate interactions without consideration of human impacts in this study, the RESFire model is capable of capturing the anthropogenic interference on fire activity and reproducing observation-based long-term trends of regional burning activity driven by climate change and human factors (Zou et al., 2019). The carbon budget variables including GPP, NEP, and NEE increase by 4%, 7%, and 33%, respectively (Fig. 7c-d). These carbon variables affect terrestrial ecosystem productivity as well as fuel load supply for biomass burning, which further modulate fire emissions that lead to discrepancies between burned area and emission changes. For instance, most decreasing changes in burned area occur in tropical and subtropical savannas and grasslands, while significant increasing changes are evident in boreal forest and tropical rainforests of Southeast Asia (Fig. 7a). This spatial shift of burning activity from low fuel loading areas (e.g., grassland) to high fuel loading areas (e.g., forest) greatly amplifies the changes in fire emissions due to boosted fuel consumption. The complex climate-fire-ecosystem interactions will be discussed in the next section.

3.3 Simulations of climate-fire-ecosystem interactions using CESM-RESFire

In the last section, we find a 19% increase of global burned area in the RCP4.5 future scenario comparing with the present-day scenario. We then examine spatial distributions and driving factors of this change in Fig. 8. The fire ignition distribution shows heterogeneous changes with significant increases in boreal forest regions over Eurasia as well as rainforest regions in South America but decreases in South American savanna and African rainforests and savanna. These changes in fire ignition are mainly driven by changes in fuel combustibility as shown by fire combustion factors (Fig. 8b), which are computed using fire weather conditions including 10-day running means of surface air temperature, precipitation, and soil moisture (Zou et al., 2019). The spatial distribution changes of fire spread (Fig. 8c) shows similar but more apparent patterns of increased fire spread rates over most regions except savanna and rainforests in Africa and South America, which are attributed to the changes in fire spread factors (Fig. 8d). These fire spread factors depend on surface temperature, relative humidity, soil wetness, and wet canopy fractions that modulate fuel moisture and fire spread rates in the model (Zou et al., 2019). The burned area changes are driven by changes of fire weather conditions affecting both fire ignition and fire spread, with a global spatial correlation coefficient of 0.4 between differences in fractional burned area (Fig. 7a) and fire counts (Fig. 8a) and of 0.38 between burned area (Fig. 7a) and fire spread rates (Fig. 8c). These burning activity changes found in this study also agree quite well with previous long-term projections based on an empirical statistical framework and a multi-model ensemble of 16 GCMs, in which they found good model agreement on increasing fire probabilities (~62%) at mid- to high-latitudes as well as decreasing fire probabilities (~20%) in the tropics (Moritz et al., 2012).

To understand the changes in specific fire weather variables, we compare the differences of surface air temperature, total precipitation rates, relative humidity, and surface wind speed between the future (CTRL2) and present-day (CTRL1) scenarios in Fig. 9. As expected in a modest warming scenario, the global annual mean temperature is projected to increase by 1.7 °C on average with pervasive warming over land areas (Fig. 9a). The temperature increases are stronger in high latitude regions like Alaska, northern Canada, and Antarctica as well as Australia. Meanwhile, hydrological conditions also undergo significant but nonhomogeneous changes in many regions in the projection, with hot and dry weather conditions favorable for fire in Australia, Southeast Asia, Central America, and the northern coast of South America (Fig. 9b and 9c). Most of these regions also show increased surface wind speed that is conducive to faster fire spread (Fig. 9d). Since these variations in fully coupled CTRL experiments can be induced by either global warming driven weather changes or fire feedback, we further decompose the total changes into two components: one without fire feedback (i.e., SENS2B-SENS1B) and the other purely by fire feedback (i.e., (CTRL2-CTRL1)-(SENS2B-SENS1B)). We show the fire induced weather changes in Fig. 10 and these without fire feedbacks in Fig. S3 in the Supplement. It is clear that the majority of the changes in fire weather conditions is driven by atmospheric conditions associated with global warming since the spatial patterns in Fig. 9 and Fig.S3 almost resemble each other over most land regions. However, fire feedbacks also exert nonnegligible effects to local and remote weather conditions that manifest as positive or negative feedback mechanisms to regional fire activities. For instance, Australia shows increased temperature (Fig. 10a) and surface wind speed (Fig. 10d), and decreased precipitation (Fig. 10b) and relative humidity (Fig. 10c) induced by fire, which are consistent with these changes without fire feedbacks (Fig. S3 in the Supplement) or the total changes (Fig. 9). In contrast, most Eurasian regions show decreased temperature (Fig.

427   10a) and increased relative humidity (Fig. 10c), with nonhomogeneous changes of precipitation (Fig. 10b) in response
428   to fire perturbations. These regionally varying results suggest complex interactions between fire and climate systems
429   that merit further investigation.

430   Therefore, we aggregate regional burned areas in each experiment and compare their changes between the two
431   scenarios to quantify regional effects of different feedback mechanisms (Fig. 11). An atmosphere-centric feedback
432   pathway is identified by comparing relative changes of regional burned area with (i.e., CTRL2-CTRL1) and without
433   (i.e., SENS2A-SENS1A) fire aerosol effects, while a vegetation-centric feedback pathway is identified by comparing
434   relative changes of regional burned area with (i.e., SENS2A-SENS1A) and without (i.e., SENS2B-SENS1B) fire
435   induced LCC. The comparison of relative changes in regional burned area with different feedback pathways reveal
436   distinct regional responses to these fire related atmospheric and vegetation processes. The most significant fire
437   feedback effects occur in North America (Fig. 11a) and South America (Fig. 11b), with the former dominated by
438   negative vegetation-centric fire feedback and the latter dominated by positive atmosphere-centric fire feedback. By
439   including fire induced LCC, the projected burned area increases over North America in the 2050s are greatly
440   suppressed and reduced from +172% in SENS2B to +94% in SENS2A and +93% in CTRL2, respectively. In contrast,
441   the burned area increases over South America considerably enlarges after incorporating fire aerosol effects in the
442   projection, from +112% in SENS2A and +113% in SENS2B to +142% in CTRL2. The fire feedback effects are also
443   evident in many other regions, such as similar positive atmosphere-centric feedbacks in Southeast Asia (Fig. 11g) and
444   Oceania (Fig. 11h) but negative atmosphere-centric feedbacks in Africa (Fig. 11e and 11f). The signs of these feedback
445   effects are determined by fire perturbation on regional fuel and fire weather conditions such as precipitation through
446   fire aerosol-cloud-precipitation interactions or changed vegetation evapotranspiration due to fire induced LCC (Fig.
447   S5 in the Supplement). It's worth noting that these feedback effects could enhance (e.g., North America and Southeast
448   Asia) or compensate (e.g., Northern Hemisphere and Southern Hemisphere Africa) each other in different regions,
449   which further increase the complexity of climate-fire-ecosystem interactions at regional and global scales. On a global
450   average, the net effect of fire feedbacks is almost neutral (Fig. 11i and Table 5) due to the offsetting between positive
451   vegetation-centric and negative atmosphere-centric feedbacks, which are largely dominated by burning activity in
452   African regions.

453   Lastly, we compare the difference of climate radiative forcing associated with these burning activity changes between
454   the future and present-day scenarios in Table 2 and Fig. 12. Due to broadly increased burning activities in the future
455   projection, fire aerosols are strongly enhanced over most fire-prone regions except Northern Hemisphere Africa and
456   South Asia (Fig. 12a), where the projected burning activity is suppressed as discussed in previous sections. Increased
457   fire aerosols lead to diverse responses in cloud liquid water path, with large increases in high-latitude regions but
458   generally decreases in the tropics and sub-tropics (Fig. 12b). These fire and weather changes result in pronounced
459   responses in radiative forcing through multiple pathways including aerosol-radiation interaction (Fig. 12c), aerosol-
460   cloud interaction (Fig. 12d), and fire induced LCC (Fig. 12e). The fire aerosol related RE changes show more
461   consistent and statistically significant changes over fire-prone regions than these induced by LCC. Previous studies
462   have suggested a net cooling effect of deforestation that could compensate for GHG waring effects on a global scale
463   (Bala et al., 2007;Jin et al., 2012;Randerson et al., 2006). Though our model captures the reduction of forest coverage

and increased springtime albedo in high-latitude regions (Fig. S6 in the Supplement), the radiative effect of fire induced LCC is almost neutral on a global basis in both present-day and future scenarios (Table 2). In general, most burning regions with increased fire aerosols show cooling effects due to enhanced aerosol scattering of solar radiation, while those with decreased fire aerosols show warming effects (Fig. 12c). Fire aerosol direct radiative forcing is overwhelmed by much stronger indirect effects through aerosol-cloud interactions (Fig. 12d), with pervasive cooling effects in high-latitude regions with increased cloudiness (Fig. 12b). Such indirect effects also dominate the net fire radiative effects at both regional and global scales, contributing to a 171% increase of global net fire radiative effect in the RCP4.5 future scenario (Table 2). This projection result is larger than the change in net fire radiative forcing based on the CCSM future projection in Ward et al. (2012), which suggested a 51% increase from -0.55 W m^{-2} in the 2000s to -0.83 W m^{-2} in the 2100s (Table 2). It is noted that their net estimate of fire radiative forcing changes includes other offline-based fire climate effects such as fire-related GHGs impacts and climate-biogeochemical cycle feedbacks, which could dampen the cooling effect of fire aerosols.

3.4 Discussion of modeling uncertainties

As discussed in previous sections, the complex climate-fire-ecosystem interactions in fire related atmospheric and vegetation processes can introduce large uncertainties in the fire projections and associated climate effects. Here we list major uncertainty sources that deserve further investigations in the future.

(1) Future projection of fire triggers such as lightning and human activity is highly uncertain and difficult to explicitly parameterize in global climate models at present. Previous studies suggested different and even contradictory changes in projected lightning in the future (Clark et al., 2017; Finney et al., 2017) due likely to the difference in lightning parameterization schemes used. Pathway dependent long-term projections of demographic data and socioeconomic conditions are also highly uncertain (Riahi et al., 2017). For these reasons, we did not consider these factors in our projection experiments by using fixed demographic and lightning data. Assessing the impacts of these factors will require implementations of different lightning parameterizations and socioeconomic scenarios in climate simulations.

(2) Similar uncertainties arise from future projections of land use and land cover changes and dynamic global vegetation modeling (DGVM). These anthropogenic and ecological processes could directly or indirectly modulate fire activities by changing fire risks and fuel availability. In this study, we used semi-static land use and land cover data with the sole consideration of fire perturbations in both historical and projection scenarios. The inclusion of DGVM will enable the projection of vegetation distributions but introduce additional uncertainties (Zou et al., 2019).

(3) The uncertainties of fire emission estimates arise from those in surface fuel loads, combustion completeness, emission factors, and vertical distributions with rising fire plumes. More measurements of these parameters over extended temporospatial scales are needed to fully evaluate these terms in the fire models. A newly developed fire plume rise scheme (Ke et al., 2019) has been recently implemented in the fire model used in this study and will be used for future fire modeling and evaluation studies.

499   (4) Last but not the least, fire aerosol radiative effects and aerosol-cloud interactions play an important role in

500   simulating the climate effects of fire aerosols. Though the atmosphere model used in this study incorporates

501   aerosol-cloud interactions, these atmospheric processes across multiple spatial and temporal scales are major

502   contributors to the uncertainties of the climate change assessments (Ciais et al., 2013; Seinfeld et al., 2016).

503   Community wide efforts are ongoing to quantify and reduce the uncertainties of climate modeling discussed

504   above.

505 **4 Conclusions and implications**

506 In this study, we conducted a series of fire-climate modeling experiments for the present-day and future scenarios with

507 explicit implementation of multiple climate-fire-ecosystem feedback mechanisms. We evaluated the CESM-RESFire

508 modeling performance in the context of fire-related radiative effects and terrestrial carbon balance. Various fire

509 radiative effects for the present-day and the RCP4.5 future scenarios are summarized in Fig. 13. We focus on radiative

510 forcing changes related with fire aerosols and fire-induced land cover change. We find an enhanced net fire radiative

511 effect, which is caused by increased global burning activity and subsequent aerosol-cloud interactions, increasing from

512 -0.59 ± 0.51 W m^{-2} in the 2000s to -1.60 ± 0.27 W m^{-2} in the 2050s. Annual global burned area and fire carbon

513 emissions increase by 19% and 100%, respectively, with large amplifications in boreal regions due to suppressed

514 precipitation and enhanced fire ignition and spread rates. These changes imply increasing fire danger over high-

515 latitude regions with prevalent peat lands, which will be more vulnerable to increased fire threats due to climate

516 change. Potential increasing burning activity in these regions may greatly increase fire carbon and tracer gas and

517 aerosol emissions that could have enormous impacts on terrestrial carbon balance and radiative budget. Our modeling

518 results imply that the increase of fire aerosols could compensate the projected decrease of anthropogenic aerosols due

519 to air pollution control policies in many regions (e.g., the eastern U.S. and China) (EPA, 2019;McClure and Jaffe,

520 2018;Wang et al., 2017;Zhao et al., 2014), where significant aerosol cooling effects dampen GHG warming effects

521 (Goldstein et al., 2009;Rosenfeld et al., 2019). Such counteractive effect to anthropogenic emission reduction would

522 also slow down air quality improvement and reduce associated health benefits revealed by previous studies

523 (Markandya et al., 2018;Zhang et al., 2018).

524 Fire aerosol emissions and fire-induced land cover change manifest two major feedback mechanisms in climate-

525 fire-ecosystem interactions, showing synergistic or antagonistic effects at regional to global scales. These two distinct

526 feedback mechanisms compete with each other and increase the complexity of interactions among each interactive

527 component. It is noted that we only included the atmosphere and land modeling components of the CESM model to

528 investigate climate effects of global fires with other major components of the earth system including the ocean and

529 sea/land ice in the prescribed data mode. Enhanced climate sensitivity and feedback and uncertainties on a multi-

530 decadal scale might be expected in a fully coupled climate modeling system as previous studies revealed (Dunne et

531 al., 2012;Dunne et al., 2013;Hazeleger et al., 2010;Andrews et al., 2012). We suggest more comprehensive evaluations

532 at regional scales to investigate these complex interactions for major fire-prone regions. More advanced fire modeling

533 capabilities are also needed by integrating additional fire-related processes and climate effects such as fire emitted

534 brown carbon (Brown et al., 2018;Feng et al., 2013;Forrister et al., 2015;Liu et al., 2015;Wang et al., 2018;Zhang et

al., 2017; Zhang et al., 2019) and fire-vegetation-climate interactions and teleconnections (Garcia et al., 2016;Stark et al., 2016). More evaluation metrics such as large wildfire extreme events should be considered in future studies to improve our understanding of global and regional fire activities, their variations and trends, and their relationship with decadal climate change.

Code and data availability

The Level-3 MODIS monthly AOD data from the Aqua platform (MYD08_M3, http://dx.doi.org/10.5067/MODIS/MYD08_M3.006) used for model evaluation are available via NASA Level-1 and Atmosphere Archive & Distribution System (LAADS) Distributed Active Archive Center (DAAC) in https://ladsweb.modaps.eosdis.nasa.gov/missions-and-measurements/products/MYD08_M3/. The AERONET Version 3 Level 2.0 AOT data are available at https://aeronet.gsfc.nasa.gov/. The GFED burned area and fire emission datasets are available at http://www.globalfiredata.org/. The CESM-RESFire simulation results of the six numerical experiments in the main text are deposited at the Figshare website (https://doi.org/10.6084/m9.figshare.9765356). The modeling source code and input data materials are available upon request, which should be addressed to Yufei Zou (yufei.zou@pnnl.gov).

Author contribution

Y. Zou and Y. Wang designed the experiments and Y. Zou carried them out. Y. Zou developed the model code and performed the simulations. Y. Zou and Y. Wang wrote the manuscript and all co-authors reviewed and edited the manuscript.

Competing interests

The authors declare that they have no conflict of interest.

Acknowledgments

This work was supported by the National Science Foundation (NSF) through grant 1243220 and by the U.S. Department of Energy (DOE)'s office of Science as part of the Regional and Global Climate Modeling Program (NSF-DOE-USDA EaSM2). The Pacific Northwest National Laboratory (PNNL) is operated for DOE by Battelle Memorial Institute under contract DE-AC05-76RL01830. H. Tian was supported by the NSF through grant 1243232. It has not been subjected to any NSF review and therefore does not necessarily reflect the views of the Foundation, and no official endorsement should be inferred.
We would like to acknowledge high-performance computing support from Cheyenne (doi:10.5065/D6RX99HX) provided by NCAR's CISL, sponsored by the National Science Foundation. We are thankful to Steve Platnick for processing the MODIS AOD data. We thank all the GFED team members for providing the GFED data at

http://www.globalfiredata.org/. We thank Wei Min Hao, Brent Holben, Paulo Artaxo, Mikhail Panchenko, Sergey Sakerin, Rachel T. Pinker and their staff for establishing and maintaining the six AERONET sites used in this study. We thank Chandan Sarangi and two anonymous reviewers for the helpful discussion to improve the presentation of this work.

References

Abatzoglou, J. T., and Williams, A. P.: Impact of anthropogenic climate change on wildfire across western US forests, P. Natl. Acad. Sci. USA, 113, 11770-11775, 10.1073/pnas.1607171113, 2016.

Abatzoglou, J. T., Williams, A. P., and Barbero, R.: Global Emergence of Anthropogenic Climate Change in Fire Weather Indices, Geophys. Res. Lett., 46, 326-336, 10.1029/2018gl080959, 2019.

Abel, S. J., Highwood, E. J., Haywood, J. M., and Stringer, M. A.: The direct radiative effect of biomass burning aerosols over southern Africa, Atmos. Chem. Phys., 5, 1999-2018, DOI 10.5194/acp-5-1999-2005, 2005.

Albani, S., Mahowald, N.M., Perry, A.T., Scanza, R.A., Zender, C.S., Heavens, N.G., Maggi, V., Kok, J.F. and Otto-Bliesner, B.L.: Improved dust representation in the Community Atmosphere Model. Journal of Advances in Modeling Earth Systems, 6, 541-570, https://doi.org/10.1002/2013MS000279, 2014.

Andela, N., Morton, D. C., Giglio, L., Chen, Y., van der Werf, G. R., Kasibhatla, P. S., DeFries, R. S., Collatz, G. J., Hantson, S., Kloster, S., Bachelet, D., Forrest, M., Lasslop, G., Li, F., Mangeon, S., Melton, J. R., Yue, C., Randerson, J. T.: A human-driven decline in global burned area, Science, 356(6345), 1356–1362. https://doi.org/10.1126/science.aal4108, 2017.

Andela, N., and van der Werf, G. R.: Recent trends in African fires driven by cropland expansion and El Nino to La Nina transition, Nature Climate Change, 4, 791–795. https://doi.org/10.1038/nclimate2313, 2014.

Andrews, T., Gregory, J. M., Webb, M. J., and Taylor, K. E.: Forcing, feedbacks and climate sensitivity in CMIP5 coupled atmosphere-ocean climate models, Geophys. Res. Lett., 39, Artn L0971210.1029/2012gl051607, 2012.

Bala, G., Caldeira, K., Wickett, M., Phillips, T. J., Lobell, D. B., Delire, C., and Mirin, A.: Combined climate and carbon-cycle effects of large-scale deforestation, P. Natl. Acad. Sci. USA, 104, 6550-6555, 10.1073/pnas.0608998104, 2007.

Barbero, R., Abatzoglou, J. T., Larkin, N. K., Kolden, C. A., and Stocks, B.: Climate change presents increased potential for very large fires in the contiguous United States, Int. J. Wildland Fire, 24, 892-899, 10.1071/Wf15083, 2015.

Bowman, D. M. J. S., Balch, J. K., Artaxo, P., Bond, W. J., Carlson, J. M., Cochrane, M. A., D'Antonio, C. M., DeFries, R. S., Doyle, J. C., Harrison, S. P., Johnston, F. H., Keeley, J. E., Krawchuk, M. A., Kull, C. A., Marston, J. B., Moritz, M. A., Prentice, I. C., Roos, C. I., Scott, A. C., Swetnam, T. W., van der Werf, G. R., and Pyne, S. J.: Fire in the Earth System, Science, 324, 481-484, 10.1126/science.1163886, 2009.

Brown, H., Liu, X. H., Feng, Y., Jiang, Y. Q., Wu, M. X., Lu, Z., Wu, C. L., Murphy, S., and Pokhrel, R.: Radiative effect and climate impacts of brown carbon with the Community Atmosphere Model (CAM5), Atmos. Chem. Phys., 18, 17745-17768, 10.5194/acp-18-17745-2018, 2018.

Ciais, P., C. Sabine, G. Bala, L. Bopp, V. Brovkin, J. Canadell, A. Chhabra, R. DeFries, J. Galloway, M. Heimann, C. Jones, C. Le Quéré, R.B. Myneni, and Thornton, S. P. a. P.: Carbon and Other Biogeochemical Cycles in Climate Change 2013: The Physical Science Basis, Cambridge, United Kingdom and New York, NY, USA, 2013.

Clarke, H., Lucas, C., and Smith, P.: Changes in Australian fire weather between 1973 and 2010, Int. J. Climatol., 33, 931-944, 10.1002/joc.3480, 2013.

Clark, S. K., Ward, D. S., and Mahowald, N. M.: Parameterization-based uncertainty in future lightning flash density, Geophys. Res. Lett., 44, 2893–2901, doi:10.1002/2017GL073017, 2017.

Computational and Information Systems Laboratory (CISL). Cheyenne: HPE/SGI ICE XA System (University Community Computing). Boulder, CO: National Center for Atmospheric Research. doi:10.5065/D6RX99HX, 2017.

Dennison, P. E., Brewer, S. C., Arnold, J. D., and Moritz, M. A.: Large wildfire trends in the western United States, 1984-2011, Geophys. Res. Lett., 41, 2928-2933, 10.1002/2014gl059576, 2014.

Dentener, F., Kinne, S., Bond, T., Boucher, O., Cofala, J., Generoso, S., Ginoux, P., Gong, S., Hoelzemann, J. J., Ito, A., Marelli, L., Penner, J. E., Putaud, J. P., Textor, C., Schulz, M., van der Werf, G. R., and Wilson, J.: Emissions of primary aerosol and precursor gases in the years 2000 and 1750 prescribed data-sets for AeroCom, Atmos. Chem. Phys., 6, 4321-4344, DOI 10.5194/acp-6-4321-2006, 2006.

Dunne, J. P., John, J. G., Adcroft, A. J., Griffies, S. M., Hallberg, R. W., Shevliakova, E., Stouffer, R. J., Cooke, W., Dunne, K. A., Harrison, M. J., Krasting, J. P., Malyshev, S. L., Milly, P. C. D., Phillipps, P. J., Sentman, L. T., Samuels, B. L., Spelman, M. J., Winton, M., Wittenberg, A. T., and Zadeh, N.: GFDL's ESM2 Global Coupled Climate-Carbon Earth System Models. Part I: Physical Formulation and Baseline Simulation Characteristics, J. Climate, 25, 6646-6665, 10.1175/Jcli-D-11-00560.1, 2012.

Dunne, J. P., John, J. G., Shevliakova, E., Stouffer, R. J., Krasting, J. P., Malyshev, S. L., Milly, P. C. D., Sentman, L. T., Adcroft, A. J., Cooke, W., Dunne, K. A., Griffies, S. M., Hallberg, R. W., Harrison, M. J., Levy, H., Wittenberg, A. T., Phillips, P. J., and Zadeh, N.: GFDL's ESM2 Global Coupled Climate-Carbon Earth System Models. Part II: Carbon System Formulation and Baseline Simulation Characteristics, J. Climate, 26, 2247-2267, 10.1175/Jcli-D-12-00150.1, 2013.

Particulate Matter (PM2.5) trends: https://www.epa.gov/air-trends/particulate-matter-pm25-trends, access: Feburary 19, 2019.

Fann, N., Alman, B., Broome, R. A., Morgan, G. G., Johnston, F. H., Pouliot, G., and Rappold, A. G.: The health impacts and economic value of wildland fire episodes in the US: 2008-2012, Sci. Total. Environ., 610, 802-809, 10.1016/j.scitotenv.2017.08.024, 2018.

Feng, Y., Ramanathan, V., and Kotamarthi, V. R.: Brown carbon: a significant atmospheric absorber of solar radiation?, Atmos. Chem. Phys., 13, 8607-8621, 10.5194/acp-13-8607-2013, 2013.

Finney, D.L., Doherty, R.M., Wild, O., Stevenson, D.S., MacKenzie, I.A. and Blyth, A.M.: A projected decrease in lightning under climate change. Nat. Clim. Change, 8, 210, https://doi.org/10.1038/s41558-018-0072-6, 2018.

Flanner, M. G., and Zender, C. S.: Snowpack radiative heating: Influence on Tibetan Plateau climate, Geophys. Res. Lett., 32, Artn L0650110.1029/2004gl022076, 2005.

637   Flannigan, M., Cantin, A. S., de Groot, W. J., Wotton, M., Newbery, A., and Gowman, L. M.: Global wildland fire
638   season severity in the 21st century, Forest Ecol. Manag., 294, 54-61, 10.1016/j.foreco.2012.10.022, 2013.

639   Flannigan, M. D., Krawchuk, M. A., de Groot, W. J., Wotton, B. M., and Gowman, L. M.: Implications of changing
640   climate for global wildland fire, Int. J. Wildland Fire, 18, 483-507, 10.1071/Wf08187, 2009.

641   Forrister, H., Liu, J., Scheuer, E., Dibb, J., Ziemba, L., Thornhill, K. L., Anderson, B., Diskin, G., Perring, A. E.,
642   Schwarz, J. P., Campuzano-Jost, P., Day, D. A., Palm, B. B., Jimenez, J. L., Nenes, A., and Weber, R. J.: Evolution
643   of brown carbon in wildfire plumes, Geophys. Res. Lett., 42, 4623-4630, 10.1002/2015gl063897, 2015.

644   Garcia, E. S., Swann, A. L. S., Villegas, J. C., Breshears, D. D., Law, D. J., Saleska, S. R., and Stark, S. C.: Synergistic
645   Ecoclimate Teleconnections from Forest Loss in Different Regions Structure Global Ecological Responses, Plos
646   One, 11, ARTN e016504210.1371/journal.pone.0165042, 2016.

647   Ghan, S. J.: Technical Note: Estimating aerosol effects on cloud radiative forcing, Atmos. Chem. Phys., 13, 9971-
648   9974, 10.5194/acp-13-9971-2013, 2013.

649   Giglio, L., Randerson, J. T., and van der Werf, G. R.: Analysis of daily, monthly, and annual burned area using the
650   fourth-generation global fire emissions database (GFED4), J. Geophys. Res.-Biogeo., 118, 317-328,
651   10.1002/jgrg.20042, 2013.

652   Gilardoni, S., Vignati, E., Marmer, E., Cavalli, F., Belis, C., Gianelle, V., Loureiro, A., and Artaxo, P.: Sources of
653   carbonaceous aerosol in the Amazon basin, Atmos. Chem. Phys., 11, 2747-2764, 10.5194/acp-11-2747-2011,
654   2011.

655   Goldstein, A. H., Koven, C. D., Heald, C. L., and Fung, I. Y.: Biogenic carbon and anthropogenic pollutants combine
656   to form a cooling haze over the southeastern United States, P. Natl. Acad. Sci. USA, 106, 8835-8840,
657   10.1073/pnas.0904128106, 2009.

658   Hall, J. R.: The total cost of fire in the United States, National Fire Protection Association, Quincy, MA, 38, 2014.

659   Hantson, S., Arneth, A., Harrison, S. P., Kelley, D. I., Prentice, I. C., Rabin, S. S., Archibald, S., Mouillot, F., Arnold,
660   S. R., Artaxo, P., Bachelet, D., Ciais, P., Forrest, M., Friedlingstein, P., Hickler, T., Kaplan, J. O., Kloster, S.,
661   Knorr, W., Lasslop, G., Li, F., Mangeon, S., Melton, J. R., Meyn, A., Sitch, S., Spessa, A., van der Werf, G. R.,
662   Voulgarakis, A., and Yue, C.: The status and challenge of global fire modelling, Biogeosciences, 13, 3359-3375,
663   10.5194/bg-13-3359-2016, 2016.

664   Harris, R. M. B., Remenyi, T. A., Williamson, G. J., Bindoff, N. L., and Bowman, D. M. J. S.: Climate-vegetation-
665   fire interactions and feedbacks: trivial detail or major barrier to projecting the future of the Earth system?, Wires
666   Clim. Change, 7, 910-931, 10.1002/wcc.428, 2016.

667   Hazeleger, W., Severijns, C., Semmler, T., Stefanescu, S., Yang, S. T., Wang, X. L., Wyser, K., Dutra, E., Baldasano,
668   J. M., Bintanja, R., Bougeault, P., Caballero, R., Ekman, A. M. L., Christensen, J. H., van den Hurk, B., Jimenez,
669   P., Jones, C., Kallberg, P., Koenigk, T., McGrath, R., Miranda, P., Van Noije, T., Palmer, T., Parodi, J. A., Schmith,
670   T., Selten, F., Storelvmo, T., Sterl, A., Tapamo, H., Vancoppenolle, M., Viterbo, P., and Willen, U.: EC-Earth A
671   Seamless Earth-System Prediction Approach in Action, B. Am. Meteorol. Soc., 91, 1357-1363,
672   10.1175/2010bams2877.1, 2010.

673   Horowitz, L.W., Walters, S., Mauzerall, D.L., Emmons, L.K., Rasch, P.J., Granier, C., Tie, X., Lamarque, J.F.,

674   Schultz, M.G., Tyndall, G.S. and Orlando, J.J.: A global simulation of tropospheric ozone and related tracers:

675   Description and evaluation of MOZART, version 2. J. Geophys. Res.-Atmos., 108, 2003.

676   Hurrell, J. W., Holland, M. M., Gent, P. R., Ghan, S., Kay, J. E., Kushner, P. J., Lamarque, J. F., Large, W. G.,

677   Lawrence, D., Lindsay, K., Lipscomb, W. H., Long, M. C., Mahowald, N., Marsh, D. R., Neale, R. B., Rasch, P.,

678   Vavrus, S., Vertenstein, M., Bader, D., Collins, W. D., Hack, J. J., Kiehl, J., and Marshall, S.: The Community

679   Earth System Model A Framework for Collaborative Research, B. Am. Meteorol. Soc., 94, 1339-1360,

680   10.1175/Bams-D-12-00121.1, 2013.

681   Hurteau, M. D., Westerling, A. L., Wiedinmyer, C., and Bryant, B. P.: Projected Effects of Climate and Development

682   on California Wildfire Emissions through 2100, Environ. Sci. Technol., 48, 2298-2304, 10.1021/es4050133, 2014.

683   Hurtt, G. C., Frolking, S., Fearon, M. G., Moore, B., Shevliakova, E., Malyshev, S., Pacala, S. W., and Houghton, R.

684   A.: The underpinnings of land-use history: three centuries of global gridded land-use transitions, wood-harvest

685   activity, and resulting secondary lands, Global Change Biol., 12, 1208-1229, 10.1111/j.1365-2486.2006.01150.x,

686   2006.

687   Jiang, Y. Q., Lu, Z., Liu, X. H., Qian, Y., Zhang, K., Wang, Y. H., and Yang, X. Q.: Impacts of global open-fire

688   aerosols on direct radiative, cloud and surface-albedo effects simulated with CAM5, Atmos. Chem. Phys., 16,

689   14805-14824, 10.5194/acp-16-14805-2016, 2016.

690   Jin, Y. F., Randerson, J. T., Goetz, S. J., Beck, P. S. A., Loranty, M. M., and Goulden, M. L.: The influence of burn

691   severity on postfire vegetation recovery and albedo change during early succession in North American boreal

692   forests, J. Geophys. Res.-Biogeo., 117, Artn G0103610.1029/2011jg001886, 2012.

693   Johnston, F. H., Henderson, S. B., Chen, Y., Randerson, J. T., Marlier, M., DeFries, R. S., Kinney, P., Bowman, D.

694   M. J. S., and Brauer, M.: Estimated Global Mortality Attributable to Smoke from Landscape Fires, Environ. Health

695   Persp., 120, 695-701, 10.1289/ehp.1104422, 2012.

696   Jolly, W. M., Cochrane, M. A., Freeborn, P. H., Holden, Z. A., Brown, T. J., Williamson, G. J., and Bowman, D. M.

697   J. S.: Climate-induced variations in global wildfire danger from 1979 to 2013, Nat. Commun., 6, ARTN

698   753710.1038/ncomms8537, 2015.

699   Ke, Z., Wang, Y., Zou, Y., Song, Y., and Liu, Y.: The global plume-rise dataset and its climate model implement,

700   submitted to J. Adv. Model Earth Sy., 2019.

701   Kloster, S., Mahowald, N. M., Randerson, J. T., Thornton, P. E., Hoffman, F. M., Levis, S., Lawrence, P. J., Feddema,

702   J. J., Oleson, K. W., and Lawrence, D. M.: Fire dynamics during the 20th century simulated by the Community

703   Land Model, Biogeosciences, 7, 1877-1902, 10.5194/bg-7-1877-2010, 2010.

704   Kloster, S., Mahowald, N. M., Randerson, J. T., and Lawrence, P. J.: The impacts of climate, land use, and demography

705   on fires during the 21st century simulated by CLM-CN, Biogeosciences, 9, 509-525, 10.5194/bg-9-509-2012,

706   2012.

707   Kurokawa, J., Ohara, T., Morikawa, T., Hanayama, S., Janssens-Maenhout, G., Fukui, T., Kawashima, K., and

708   Akimoto, H.: Emissions of air pollutants and greenhouse gases over Asian regions during 2000-2008: Regional

Emission inventory in ASia (REAS) version 2, Atmos. Chem. Phys., 13, 11019-11058, 10.5194/acp-13-11019-2013, 2013.

Lamarque, J. F., Bond, T. C., Eyring, V., Granier, C., Heil, A., Klimont, Z., Lee, D., Liousse, C., Mieville, A., Owen, B., Schultz, M. G., Shindell, D., Smith, S. J., Stehfest, E., Van Aardenne, J., Cooper, O. R., Kainuma, M., Mahowald, N., McConnell, J. R., Naik, V., Riahi, K., and van Vuuren, D. P.: Historical (1850-2000) gridded anthropogenic and biomass burning emissions of reactive gases and aerosols: methodology and application, Atmos. Chem. Phys., 10, 7017-7039, 10.5194/acp-10-7017-2010, 2010.

Le Quere, C., Andres, R. J., Boden, T., Conway, T., Houghton, R. A., House, J. I., Marland, G., Peters, G. P., van der Werf, G. R., Ahlstrom, A., Andrew, R. M., Bopp, L., Canadell, J. G., Ciais, P., Doney, S. C., Enright, C., Friedlingstein, P., Huntingford, C., Jain, A. K., Jourdain, C., Kato, E., Keeling, R. F., Goldewijk, K. K., Levis, S., Levy, P., Lomas, M., Poulter, B., Raupach, M. R., Schwinger, J., Sitch, S., Stocker, B. D., Viovy, N., Zaehle, S., and Zeng, N.: The global carbon budget 1959-2011, Earth Syst. Sci. Data, 5, 165-185, 10.5194/essd-5-165-2013, 2013.

Li, F., Levis, S., and Ward, D. S.: Quantifying the role of fire in the Earth system - Part 1: Improved global fire modeling in the Community Earth System Model (CESM1), Biogeosciences, 10, 2293-2314, 10.5194/bg-10-2293-2013, 2013.

Li, F., Bond-Lamberty, B., and Levis, S.: Quantifying the role of fire in the Earth system - Part 2: Impact on the net carbon balance of global terrestrial ecosystems for the 20th century, Biogeosciences, 11, 1345-1360, 10.5194/bg-11-1345-2014, 2014.

Liu, J., Scheuer, E., Dibb, J., Diskin, G. S., Ziemba, L. D., Thornhill, K. L., Anderson, B. E., Wisthaler, A., Mikoviny, T., Devi, J. J., Bergin, M., Perring, A. E., Markovic, M. Z., Schwarz, J. P., Campuzano-Jost, P., Day, D. A., Jimenez, J. L., and Weber, R. J.: Brown carbon aerosol in the North American continental troposphere: sources, abundance, and radiative forcing, Atmos. Chem. Phys., 15, 7841-7858, 10.5194/acp-15-7841-2015, 2015.

Liu, X., Easter, R. C., Ghan, S. J., Zaveri, R., Rasch, P., Shi, X., Lamarque, J. F., Gettelman, A., Morrison, H., Vitt, F., Conley, A., Park, S., Neale, R., Hannay, C., Ekman, A. M. L., Hess, P., Mahowald, N., Collins, W., Iacono, M. J., Bretherton, C. S., Flanner, M. G., and Mitchell, D.: Toward a minimal representation of aerosols in climate models: description and evaluation in the Community Atmosphere Model CAM5, Geosci. Model Dev., 5, 709-739, 10.5194/gmd-5-709-2012, 2012.

Liu, Y., Zhang, K., Qian, Y., Wang, Y., Zou, Y., Song, Y., Wan, H., Liu, X., and Yang, X.-Q.: Investigation of short-term effective radiative forcing of fire aerosols over North America using nudged hindcast ensembles, Atmos. Chem. Phys., 18, 31-47, 10.5194/acp-18-31-2018, 2018.

Liu, Y. Q.: New development and application needs for Earth system modeling of fire-climate-ecosystem interactions, Environ. Res. Lett., 13, ARTN 01100110.1088/1748-9326/aaa347, 2018.

Liu, Y. Q., Stanturf, J., and Goodrick, S.: Trends in global wildfire potential in a changing climate, Forest Ecol. Manag., 259, 685-697, 10.1016/j.foreco.2009.09.002, 2010.

744 Lu, Z., Liu, X., Zhang, Z., Zhao, C., Meyer, K., Rajapakshe, C., Wu, C., Yang, Z. and Penner, J.E.: Biomass smoke
745   from southern Africa can significantly enhance the brightness of stratocumulus over the southeastern Atlantic
746   Ocean. Proc. Natl. Acad. Sci. U.S.A., 115, 2924-2929, https://doi.org/10.1073/pnas.1713703115, 2018.

747 Markandya, A., Sampedro, J., Smith, S. J., Dingenen, R. V., Pizarro-Irizar, C., Arto, I., and González-Eguino, M.:
748   Health co-benefits from air pollution and mitigation costs of the Paris Agreement: a modelling study, The Lancet
749   Planetary Health, 2, e126-e133, https://doi.org/10.1016/S2542-5196(18)30029-9, 2018.

750 Martin, M. V., Logan, J. A., Kahn, R. A., Leung, F. Y., Nelson, D. L., and Diner, D. J.: Smoke injection heights from
751   fires in North America: analysis of 5 years of satellite observations, Atmos. Chem. Phys., 10, 1491-1510, 2010.

752 McClure, C. D., and Jaffe, D. A.: US particulate matter air quality improves except in wildfire-prone areas, P. Natl.
753   Acad. Sci. USA, 115, 7901-7906, 10.1073/pnas.1804353115, 2018.

754 Moritz, M. A., Parisien, M. A., Batllori, E., Krawchuk, M. A., Van Dorn, J., Ganz, D. J., and Hayhoe, K.: Climate
755   change and disruptions to global fire activity, Ecosphere, 3, Unsp 4910.1890/Es11-00345.1, 2012.

756 Neale, R. B., Chen, C. C., Gettelman, A., Lauritzen, P. H., Park, S., Williamson, D. L., Conley, A. J., Garcia, R.,
757   Kinnison, D., Lamarque, J. F., Marsh, D., Mills, M., Smith, A. K., Tilmes, S., Vitt, F., Morrison, H., Cameron-
758   Smith, P., Collins, W. D., Iacono, M. J., Easter, R. C., Ghan, S. J., Liu, X. H., Rasch, P. J., and Taylor, M. A.:
759   Description of the NCAR Community Atmosphere Model (CAM 5.0), NCAR 289, 2013.

760 Oleson, K. W., Lawrence, D. M., Bonan, G. B., Drewniak, B., Huang, M., Koven, C. D., Levis, S., Li, F., Riley, W.
761   J., Subin, Z. M., Swenson, S. C., Thornton, P. E., Bozbiyik, A., Fisher, R., Heald, C. L., Kluzek, E., Lamarque, J.-
762   F., Lawrence, P. J., Leung, L. R., Lipscomb, W., Muszala, S., Ricciuto, D. M., Sacks, W., Sun, Y., Tang, J., and
763   Yang, Z.-L.: Technical description of version 4.5 of the Community Land Model (CLM), NCAR 434, 2013.

764 Park, S., Bretherton, C. S., and Rasch, P. J.: Integrating Cloud Processes in the Community Atmosphere Model,
765   Version 5, J. Climate, 27, 6821-6856, 10.1175/Jcli-D-14-00087.1, 2014.

766 Parks, S. A., Miller, C., Abatzoglou, J. T., Holsinger, L. M., Parisien, M. A., and Dobrowski, S. Z.: How will climate
767   change affect wildland fire severity in the western US?, Environ. Res. Lett., 11, Artn 03500210.1088/1748-
768   9326/11/3/035002, 2016.

769 Pellegrini, A. F. A., Ahlstrom, A., Hobbie, S. E., Reich, P. B., Nieradzik, L. P., Staver, A. C., Scharenbroch, B. C.,
770   Jumpponen, A., Anderegg, W. R. L., Randerson, J. T., and Jackson, R. B.: Fire frequency drives decadal changes
771   in soil carbon and nitrogen and ecosystem productivity, Nature, 553, 194-198, 10.1038/nature24668, 2018.

772 Piao, S. L., Sitch, S., Ciais, P., Friedlingstein, P., Peylin, P., Wang, X. H., Ahlstrom, A., Anav, A., Canadell, J. G.,
773   Cong, N., Huntingford, C., Jung, M., Levis, S., Levy, P. E., Li, J. S., Lin, X., Lomas, M. R., Lu, M., Luo, Y. Q.,
774   Ma, Y. C., Myneni, R. B., Poulter, B., Sun, Z. Z., Wang, T., Viovy, N., Zaehle, S., and Zeng, N.: Evaluation of
775   terrestrial carbon cycle models for their response to climate variability and to CO2 trends, Global Change Biol.,
776   19, 2117-2132, 10.1111/gcb.12187, 2013.

777 Quillet, A., Peng, C, Garneau, M.: Toward dynamic global vegetation models for simulating vegetation–climate
778   interactions and feedbacks: recent developments, limitations, and future challenges, Environmental Reviews,
779   18(NA), 333-53, 10.1139/A10-016, 2010.

780   Randerson, J. T., Liu, H., Flanner, M. G., Chambers, S. D., Jin, Y., Hess, P. G., Pfister, G., Mack, M. C., Treseder, K.
781   K., Welp, L. R., Chapin, F. S., Harden, J. W., Goulden, M. L., Lyons, E., Neff, J. C., Schuur, E. A. G., and Zender,
782   C. S.: The impact of boreal forest fire on climate warming, Science, 314, 1130-1132, 10.1126/science.1132075,
783   2006.
784   Randerson, J. T., Chen, Y., van der Werf, G. R., Rogers, B. M., and Morton, D. C.: Global burned area and biomass
785   burning emissions from small fires, J. Geophys. Res.-Biogeo., 117, Artn G0401210.1029/2012jg002128, 2012.
786   Rayner, N. A., Parker, D. E., Horton, E. B., Folland, C. K., Alexander, L. V., Rowell, D. P., Kent, E. C., and Kaplan,
787   A.: Global analyses of sea surface temperature, sea ice, and night marine air temperature since the late nineteenth
788   century, J. Geophys. Res.-Atmos., 108, Artn 440710.1029/2002jd002670, 2003.
789   Riahi, K., Van Vuuren, D.P., Kriegler, E., Edmonds, J., O'neill, B.C., Fujimori, S., Bauer, N., Calvin, K., Dellink, R.,
790   Fricko, O. and Lutz, W.: The shared socioeconomic pathways and their energy, land use, and greenhouse gas
791   emissions   implications: an   overview.   Global   Environmental   Change,   42,   153-168,
792   http://dx.doi.org/10.1016/j.gloenvcha.2016.05.009, 2017.
793   Platnick, S., Hubanks, P., Meyer, K., and King, M. D.: MODIS Atmosphere L3 Monthly Product. NASA MODIS
794   Adaptive   Processing   System,   Goddard   Space   Flight   Center,   USA:
795   http://dx.doi.org/10.5067/MODIS/MYD08_M3.061, 2015.
796   Richardson, L. A., Champ, P. A., and Loomis, J. B.: The hidden cost of wildfires: Economic valuation of health effects
797   of wildfire smoke exposure in Southern California, J. Forest. Econ., 18, 14-35, 10.1016/j.jfe.2011.05.002, 2012.
798   Rosenfeld, D., Zhu, Y. N., Wang, M. H., Zheng, Y. T., Goren, T., and Yu, S. C.: Aerosol-driven droplet concentrations
799   dominate   coverage   and   water   of   oceanic   low-level   clouds,   Science,   363,   599-+,   ARTN
800   eaav056610.1126/science.aav0566, 2019.
801   Seidl, R., Thom, D., Kautz, M., Martin-Benito, D., Peltoniemi, M., Vacchiano, G., Wild, J., Ascoli, D., Petr, M.,
802   Honkaniemi, J., Lexer, M. J., Trotsiuk, V., Mairota, P., Svoboda, M., Fabrika, M., Nagel, T. A., and Reyer, C. P.
803   O.: Forest disturbances under climate change, Nat. Clim. Change, 7, 395-402, 10.1038/Nclimate3303, 2017.
804   Seinfeld, J.H., Bretherton, C., Carslaw, K.S., Coe, H., DeMott, P.J., Dunlea, E.J., Feingold, G., Ghan, S., Guenther,
805   A.B., Kahn, R. and Kraucunas, I.: Improving our fundamental understanding of the role of aerosol−cloud
806   interactions in the climate system. Proc. Natl. Acad. Sci. U.S.A., 113, 5781-5790, 2016.
807   Seo, H., and Kim, Y.: Interactive impacts of fire and vegetation dynamics on global carbon and water budget using
808   Community Land Model version 4.5, Geosci. Model. Dev., 12, 457-472, 10.5194/gmd-12-457-2019, 2019.
809   Shuman, J. K., Foster, A. C., Shugart, H. H., Hoffman-Hall, A., Krylov, A., Loboda, T., Ershov, D., and Sochilova,
810   E.: Fire disturbance and climate change: implications for Russian forests, Environ. Res. Lett., 12, ARTN
811   03500310.1088/1748-9326/aa5eed, 2017.
812   Sofiev, M., Ermakova, T., and Vankevich, R.: Evaluation of the smoke-injection height from wild-land fires using
813   remote-sensing data, Atmos. Chem. Phys., 12, 1995-2006, 10.5194/acp-12-1995-2012, 2012.
814   Stark, S. C., Breshears, D. D., Garcia, E. S., Law, D. J., Minor, D. M., Saleska, S. R., Swann, A. L. S., Villegas, J. C.,
815   Aragao, L. E. O. C., Bella, E. M., Borma, L. S., Cobb, N. S., Litvak, M. E., Magnusson, W. E., Morton, J. M., and

816   Redmond, M. D.: Toward accounting for ecoclimate teleconnections: intra- and inter-continental consequences of
817   altered energy balance after vegetation change, Landscape Ecol., 31, 181-194, 10.1007/s10980-015-0282-5, 2016.

818 Sun, Y., Gu, L. H., and Dickinson, R. E.: A numerical issue in calculating the coupled carbon and water fluxes in a
819   climate model, J. Geophys. Res.-Atmos., 117, Artn D2210310.1029/2012jd018059, 2012.

820 Thomas, D., Butry, D., Gilbert, S., Webb, D., and Fung, J.: The costs and losses of wildfires: A literature review,
821   National Institute of Standards and Technology, 72, 2017.

822 Thonicke, K., Spessa, A., Prentice, I. C., Harrison, S. P., Dong, L., and Carmona-Moreno, C.: The influence of
823   vegetation, fire spread and fire behaviour on biomass burning and trace gas emissions: results from a process-
824   based model, Biogeosciences, 7, 1991-2011, 10.5194/bg-7-1991-2010, 2010.

825 Tosca, M. G., Randerson, J. T., and Zender, C. S.: Global impact of smoke aerosols from landscape fires on climate
826   and the Hadley circulation, Atmos. Chem. Phys., 13, 5227-5241, 10.5194/acp-13-5227-2013, 2013.

827 Tost, H., Jöckel, P., and Lelieveld, J.: Lightning and convection parameterisations – uncertainties in global modelling,
828   Atmos. Chem. Phys., 7, 4553–4568, https://doi.org/10.5194/acp-7-4553-2007, 2007.

829 van der Werf, G. R., Randerson, J. T., Giglio, L., Collatz, G. J., Kasibhatla, P. S., and Arellano, A. F.: Interannual
830   variability in global biomass burning emissions from 1997 to 2004, Atmos. Chem. Phys., 6, 3423-3441, DOI
831   10.5194/acp-6-3423-2006, 2006.

832 van der Werf, G. R., Randerson, J. T., Giglio, L., van Leeuwen, T. T., Chen, Y., Rogers, B. M., Mu, M. Q., van Marle,
833   M. J. E., Morton, D. C., Collatz, G. J., Yokelson, R. J., and Kasibhatla, P. S.: Global fire emissions estimates
834   during 1997-2016, Earth Syst. Sci. Data, 9, 697-720, 10.5194/essd-9-697-2017, 2017.

835 Wang, J. D., Zhao, B., Wang, S. X., Yang, F. M., Xing, J., Morawska, L., Ding, A. J., Kulmala, M., Kerminen, V. M.,
836   Kujansuu, J., Wang, Z. F., Ding, D. A., Zhang, X. Y., Wang, H. B., Tian, M., Petaja, T., Jiang, J. K., and Hao, J.
837   M.: Particulate matter pollution over China and the effects of control policies, Sci. Total Environ., 584, 426-447,
838   10.1016/j.scitotenv.2017.01.027, 2017.

839 Wang, X., Heald, C. L., Liu, J. M., Weber, R. J., Campuzano-Jost, P., Jimenez, J. L., Schwarz, J. P., and Perring, A.
840   E.: Exploring the observational constraints on the simulation of brown carbon, Atmos. Chem. Phys., 18, 635-653,
841   10.5194/acp-18-635-2018, 2018.

842 Ward, D. S., Kloster, S., Mahowald, N. M., Rogers, B. M., Randerson, J. T., and Hess, P. G.: The changing radiative
843   forcing of fires: global model estimates for past, present and future, Atmos. Chem. Phys., 12, 10857-10886,
844   10.5194/acp-12-10857-2012, 2012.

845 Westerling, A. L., Hidalgo, H. G., Cayan, D. R., and Swetnam, T. W.: Warming and earlier spring increase western
846   US forest wildfire activity, Science, 313, 940-943, 10.1126/science.1128834, 2006.

847 Wotton, B. M., Flannigan, M. D., and Marshall, G. A.: Potential climate change impacts on fire intensity and key
848   wildfire suppression thresholds in Canada, Environ. Res. Lett., 12, ARTN 09500310.1088/1748-9326/aa7e6e,
849   2017.

850 Yang, G., Di, X. Y., Guo, Q. X., Shu, Z., Zeng, T., Yu, H. Z., and Wang, C.: The impact of climate change on forest
851   fire danger rating in China's boreal forest, J. For. Res., 22, 249-257, 10.1007/s11676-011-0158-8, 2011.

852   Yang, J., Tian, H. Q., Tao, B., Ren, W., Pan, S. F., Liu, Y. Q., and Wang, Y. H.: A growing importance of large fires
853   in conterminous United States during 1984-2012, J. Geophys. Res.-Biogeo., 120, 2625-2640,
854   10.1002/2015jg002965, 2015.

855   Young, A. M., Higuera, P. E., Duffy, P. A., and Hu, F. S.: Climatic thresholds shape northern high-latitude fire regimes
856   and imply vulnerability to future climate change, Ecography., 40, 606-617, 10.1111/ecog.02205, 2017.

857   Yue, C., Ciais, P., Cadule, P., Thonicke, K., and van Leeuwen, T. T.: Modelling the role of fires in the terrestrial
858   carbon balance by incorporating SPITFIRE into the global vegetation model ORCHIDEE - Part 2: Carbon
859   emissions and the role of fires in the global carbon balance, Geosci. Model Dev., 8, 1321-1338, 10.5194/gmd-8-
860   1321-2015, 2015.

861   Yue, C., Ciais, P., Zhu, D., Wang, T., Peng, S. S., and Piao, S. L.: How have past fire disturbances contributed to the
862   current carbon balance of boreal ecosystems?, Biogeosciences, 13, 675-690, 10.5194/bg-13-675-2016, 2016.

863   Yue, X., Mickley, L. J., Logan, J. A., and Kaplan, J. O.: Ensemble projections of wildfire activity and carbonaceous
864   aerosol concentrations over the western United States in the mid-21st century, Atmos. Environ., 77, 767-780,
865   10.1016/j.atmosenv.2013.06.003, 2013.

866   Zhang, A., Wang, Y., Zhang, Y., Weber, R. J., Song, Y., Ke, Z., and Zou, Y.: Modeling global radiative effect of
867   brown carbon: A larger heating source in the tropical free troposphere than black carbon, Atmos. Chem. Phys.
868   Discuss., https://doi.org/10.5194/acp-2019-594, in review, 2019.

869   Zhang, Y., West, J. J., Mathur, R., Xing, J., Hogrefe, C., Roselle, S. J., Bash, J. O., Pleim, J. E., Gan, C.-M., and
870   Wong, D. C.: Long-term trends in the ambient $PM_{2.5}$- and O_3-related mortality burdens in the United States under
871   emission reductions from 1990 to 2010, Atmos. Chem. Phys., 18, 15003-15016, https://doi.org/10.5194/acp-18-
872   15003-2018, 2018.

873   Zhang, Y. Z., Forrister, H., Liu, J. M., Dibb, J., Anderson, B., Schwarz, J. P., Perring, A. E., Jimenez, J. L.,
874   Campuzano-Jost, P., Wang, Y. H., Nenes, A., and Weber, R. J.: Top-of-atmosphere radiative forcing affected by
875   brown carbon in the upper troposphere, Nat. Geosci., 10, 486-+, 10.1038/Ngeo2960, 2017.

876   Zhang, Z., Meyer, K., Yu, H., Platnick, S., Colarco, P., Liu, Z., and Oreopoulos, L.: Shortwave direct radiative effects
877   of above-cloud aerosols over global oceans derived from 8 years of CALIOP and MODIS observations, Atmos.
878   Chem. Phys., 16, 2877-2900, 10.5194/acp-16-2877-2016, 2016.

879   Zhao, M. S., Heinsch, F. A., Nemani, R. R., and Running, S. W.: Improvements of the MODIS terrestrial gross and
880   net primary production global data set, Remote Sens. Environ., 95, 164-176, 10.1016/j.rse.2004.12.011, 2005.

881   Zhao, M. S., and Running, S. W.: Drought-Induced Reduction in Global Terrestrial Net Primary Production from 2000
882   Through 2009, Science, 329, 940-943, 10.1126/science.1192666, 2010.

883   Zhao, Y., Zhang, J., and Nielsen, C. P.: The effects of energy paths and emission controls and standards on future
884   trends in China's emissions of primary air pollutants, Atmos. Chem. Phys., 14, 8849-8868, 10.5194/acp-14-8849-
885   2014, 2014.

886   Zou, Y., Wang, Y., Ke, Z., Tian, H., Yang, J., and Liu, Y.: Development of a REgion-Specific ecosystem feedback
887   Fire (RESFire) model in the Community Earth System Model, J. Adv. Model Earth Sy.,
888   https://doi.org/10.1029/2018MS001368, 2019

889
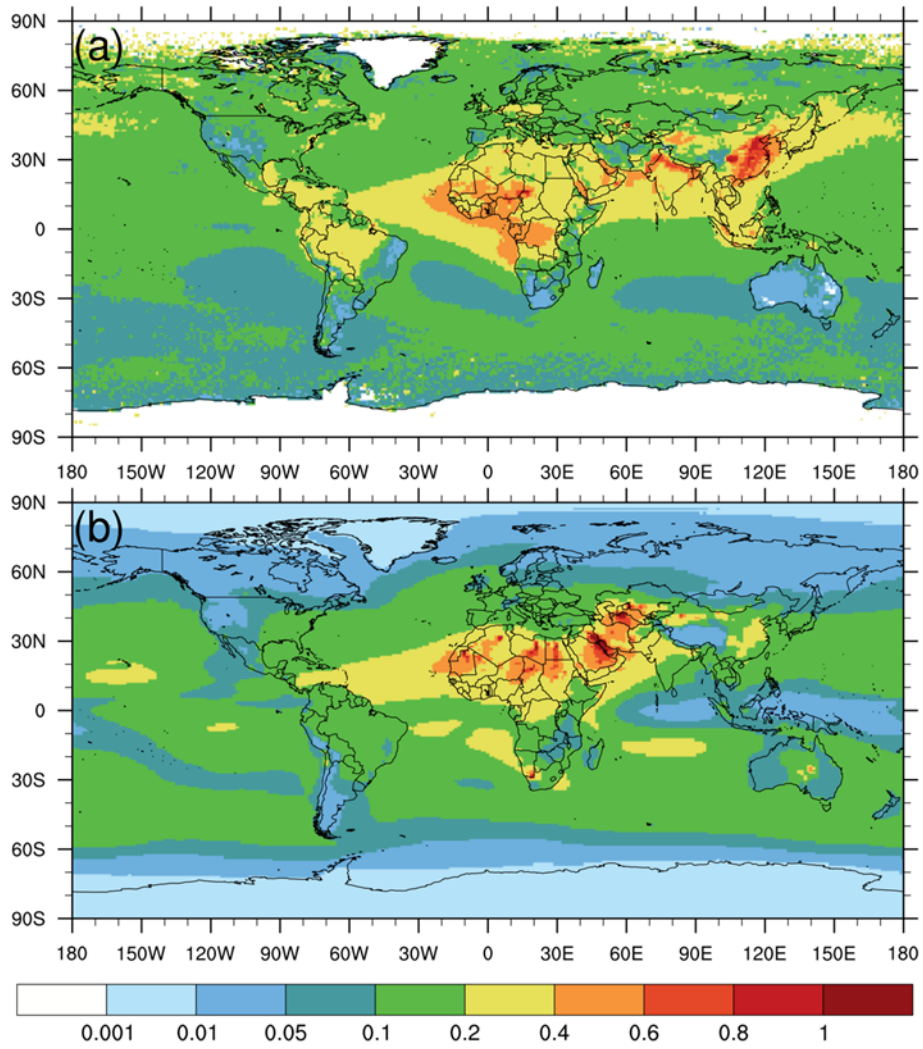
Figure 1: Comparison of annual averaged column AOD at 550 nm from (a) MODIS aboard the Aqua satellite (2003-2010);

(b) CAM5 simulation averaged from 2001 to 2010.

892
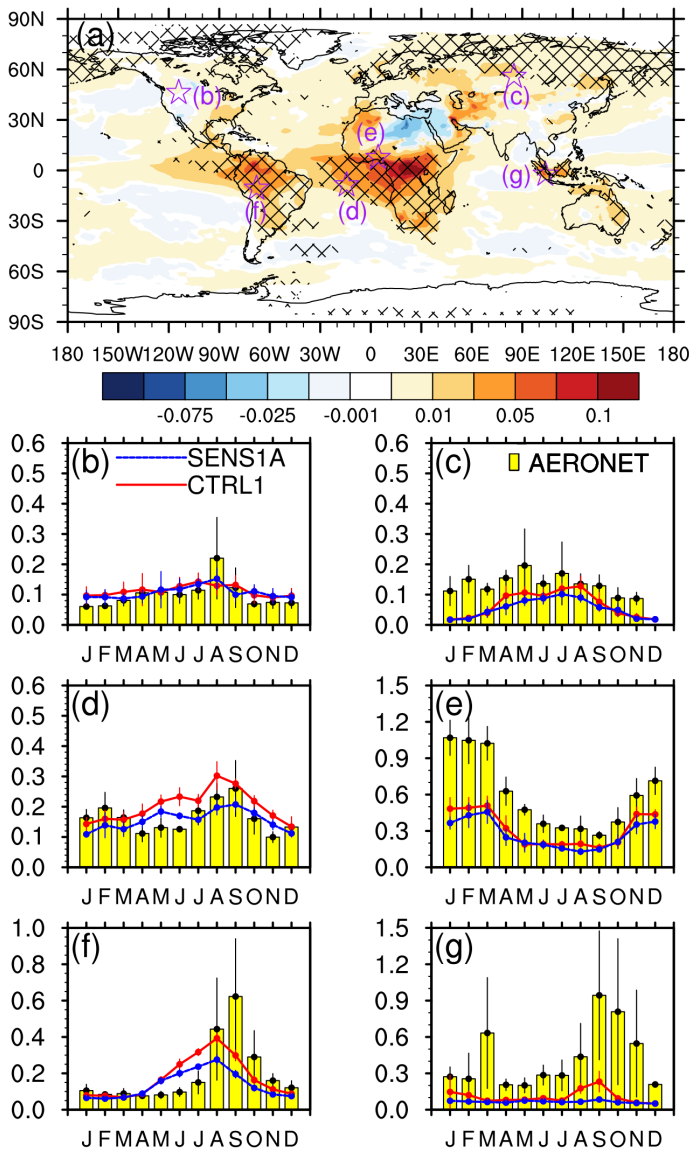
Figure 2: CESM-RESFire simulation of (a) annual averaged fire contributed AOD at 550 nm (shading) in the present-day scenario (CTRL1-SENS1A). The stars denote the AERONET site location and the hatchings denote the 0.05 significance level of the two-tailed Student's t-test; (b) comparison with AERONET monthly AOT observations at 550 nm in Missoula (114.1°W, 46.9°N) during the 2000s. The error bars denote ±1 standard deviations of interannual variations in the simulations and observations, respectively.; (c) same as (b) but in Tomsk (85.1°E, 56.5°N); (d) same as (b) but in Ascension island (14.4°W, 8.0°S); (e) same as (b) but in Ilorin (4.3°E, 8.3°N); (f) same as (b) but in Rio Branco (67.9°W, 10.0°S); (g) same as (b) but in Jambi (103.6°E, 1.6°S).
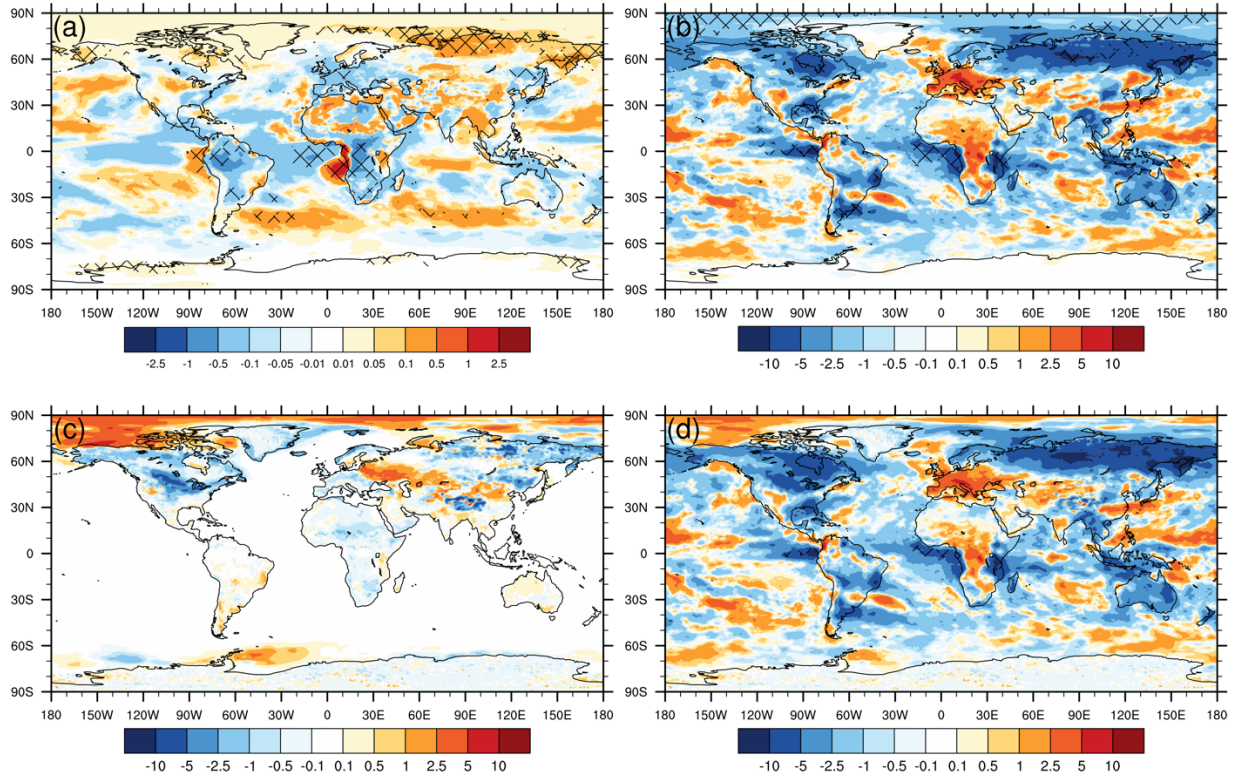
Figure 3: Present-day simulation of fire contributed annual averaged radiative effects through (a) aerosol-radiation interactions (RE$_{ari}$, W m^{-2}); (b) aerosol-cloud interactions (RE$_{aci}$, W m^{-2}); (c) fire aerosol-induced surface albedo change (RE$_{sac}$, W m^{-2}); (d) fire aerosol-related net radiative effects (RE$_{aer}$, W m^{-2}). All these radiative effects are estimated as changes in the shortwave radiative flux at the TOA between CTRL1 and SENS1A experiments. The hatchings denote the 0.05 significance level.

906
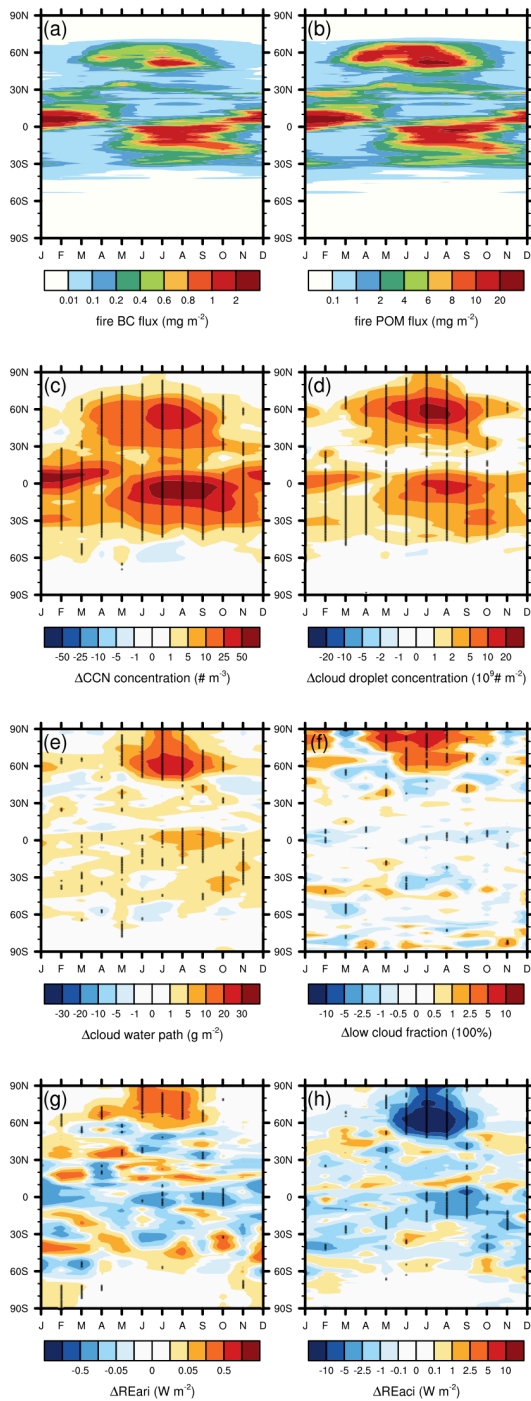
907 **Figure 4: Present-day simulation of zonal averaged time-latitude cross sections of (a) monthly BC fire emission fluxes (mg**

908 **m⁻²) in CTRL1; (b) monthly POM fire emission fluxes (mg m⁻²) in CTRL1; (c) fire-induced low-level (averaged below 800**

909 **hPa) cloud condensation nuclei (CCN, # m⁻³) concentration changes (CTRL1-SENS1A); (d) vertically-integrated cloud**

910 **droplet number concentration (CDNUMC, 10^9# m⁻²) changes (CTRL1-SENS1A); (e) cloud water path (CWP, g m⁻²) changes**

911 **(CTRL1-SENS1A); (f) low cloud cover fraction (100%) changes (CTRL1-SENS1A); (g) radiative effect changes (CTRL1-**

912 **SENS1A) by fire aerosol-radiation interactions (RE_ari , W m⁻²); (h) radiative effect changes (CTRL1-SENS1A) by fire**

913 **aerosol-cloud interactions (RE_aci , W m⁻²). The dots in (c)-(h) denote the 0.05 significance level.**

914

Figure 5: Comparison of CESM-RESFire simulated annual median injection heights (m) of fire plumes in the (a) present-day (CTRL1) and (b) RCP4.5 (CTRL2) scenarios. The inlets show statistical distributions of all plume injection heights in model grid cells of each scenario.

918
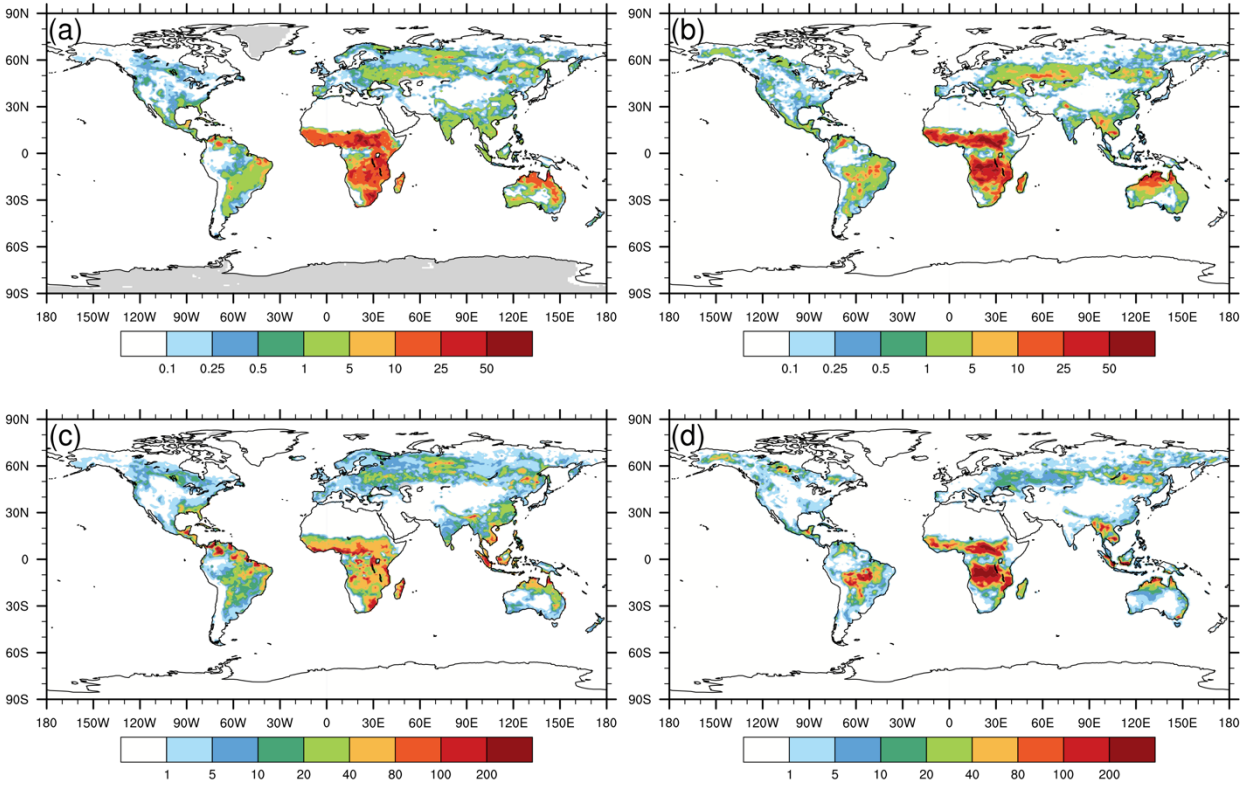
919 **Figure 6: Comparison of CESM-RESFire simulations and GFED4.1s data. (a) ensemble averaged annual fractional burned**

920 **area (% yr^{-1}) simulation; (b) 10-year averaged (2001-2010) annual fractional burned area (% yr^{-1}) based on the GFED4.1s**

921 **data; (c) ensemble averaged annual fire carbon emission (gC m^{-2} yr^{-1}) simulation; (d) 10-year averaged (2001-2010) annual**

922 **fire carbon emission (gC m^{-2} yr^{-1}) based on the GFED4.1s data.**
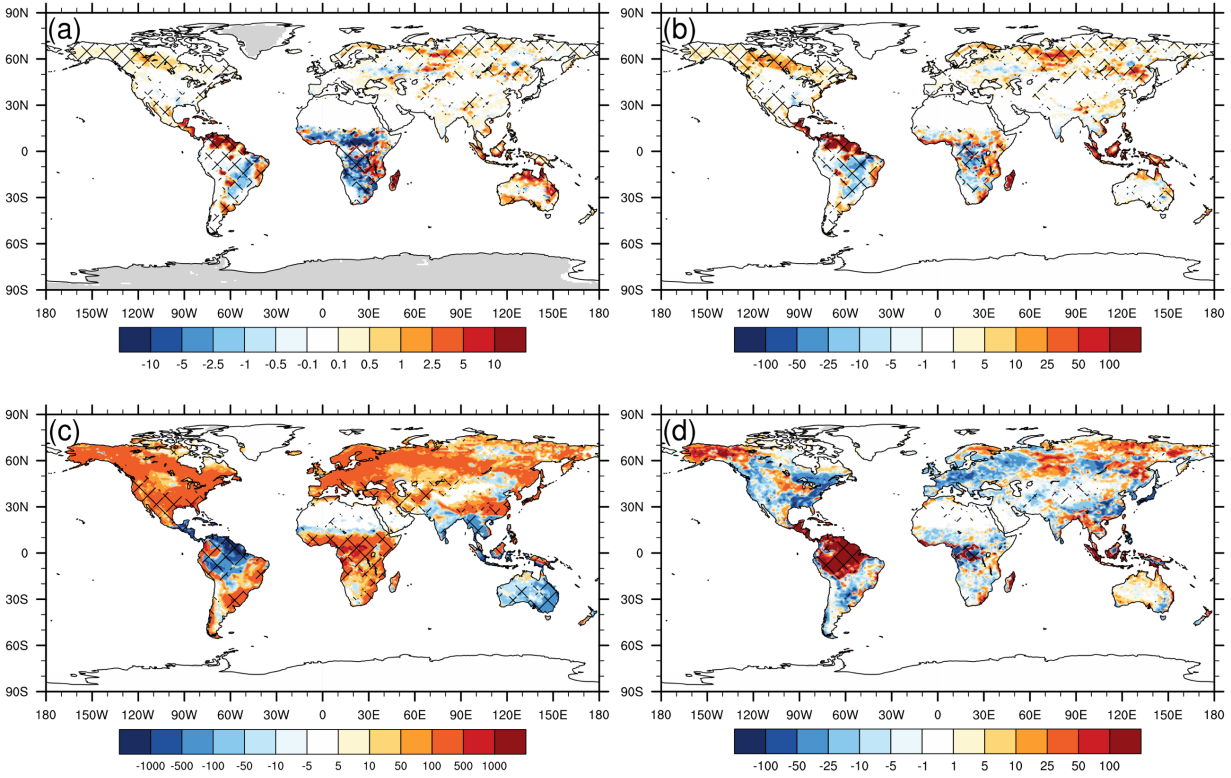
Figure 7: CESM-RESFire simulated changes between the RCP4.5 future scenario and the present-day scenario (CTRL2-CTRL1) in (a) annual fractional burned area (% yr^{-1}); (b) annual averaged fire carbon emissions (gC m^{-2} yr^{-1}); (c) annual averaged GPP (gC m^{-2} yr^{-1}); (d) annual averaged NEE (gC m^{-2} yr^{-1}). The hatchings denote the 0.05 significance level.

928
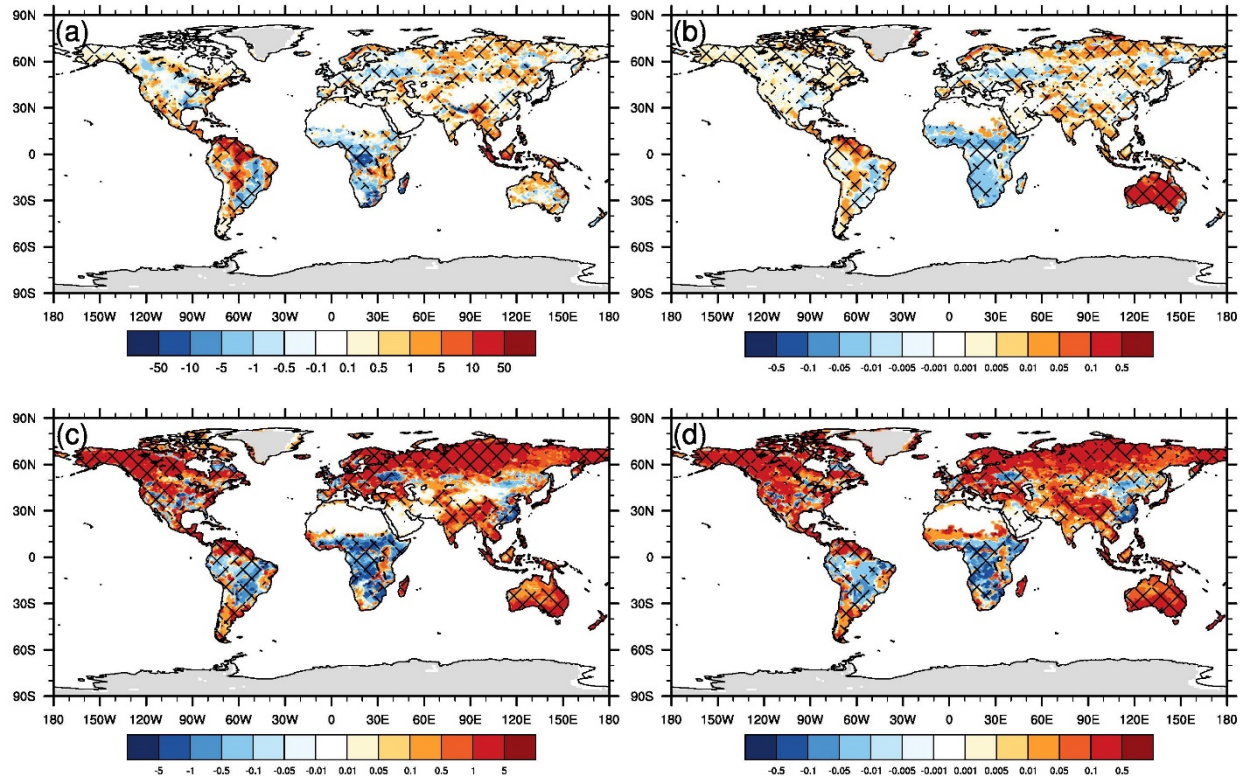
Figure 8: CESM-RESFire simulated changes in fire-related variables between the RCP4.5 future scenario and the present-day scenario (CTRL2-CTRL1). (a) changes in annual total fire ignition (NFIRE, 1E-3 count km^{-2} yr^{-1}); (b) changes in annual averaged fire combustion factors (FCF, unitless); (c) changes in annual averaged fire spread rates (FSR_DW, cm s^{-1}); (d) changes in annual averaged fire spread factors (FSF, unitless). The hatchings denote the 0.05 significance level.
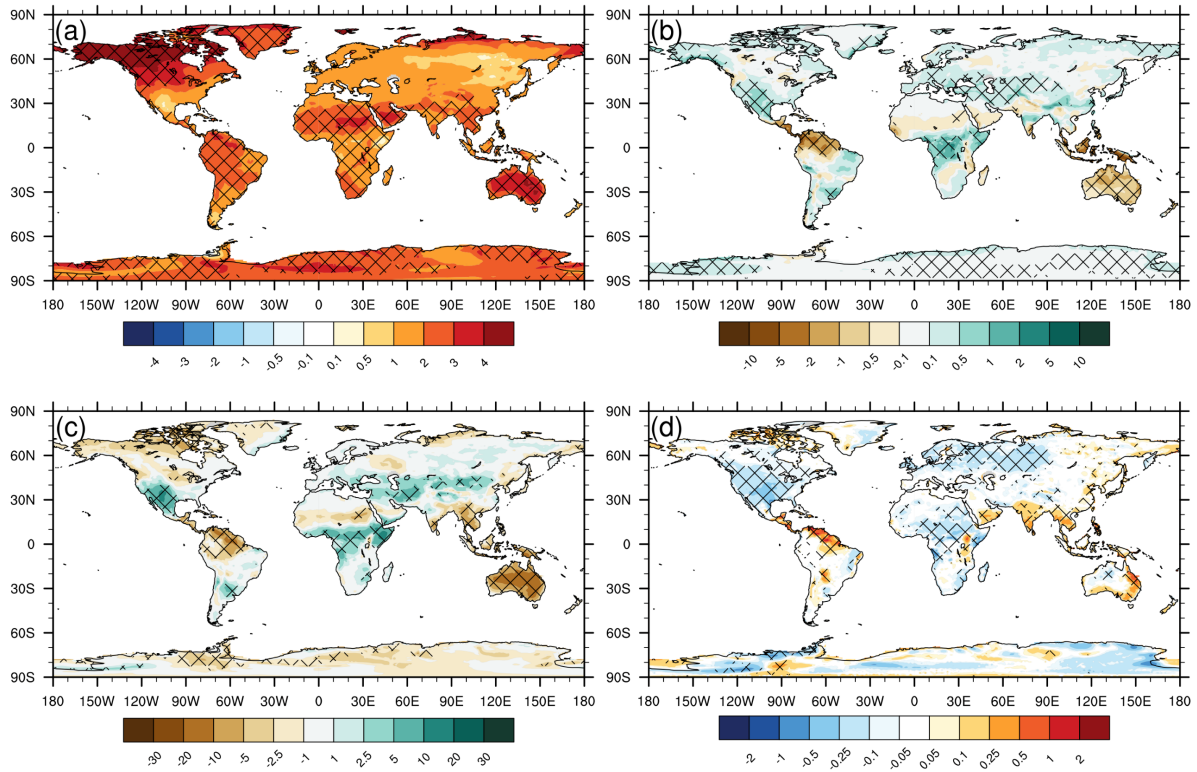
Figure 9: CESM-RESFire simulated changes in fire weather variables between the RCP4.5 future scenario and the present-day scenario (CTRL2-CTRL1). (a) changes in surface temperature (K); (b) changes in total precipitation rate (mm day^{-1}); (c) changes in surface relative humidity (%); (d) changes in surface wind speed (m s^{-1}). The hatchings denote the 0.05 significance level. For clear comparison with fire changes in Fig. 7 and 8, only fire weather changes over land are shown.

938
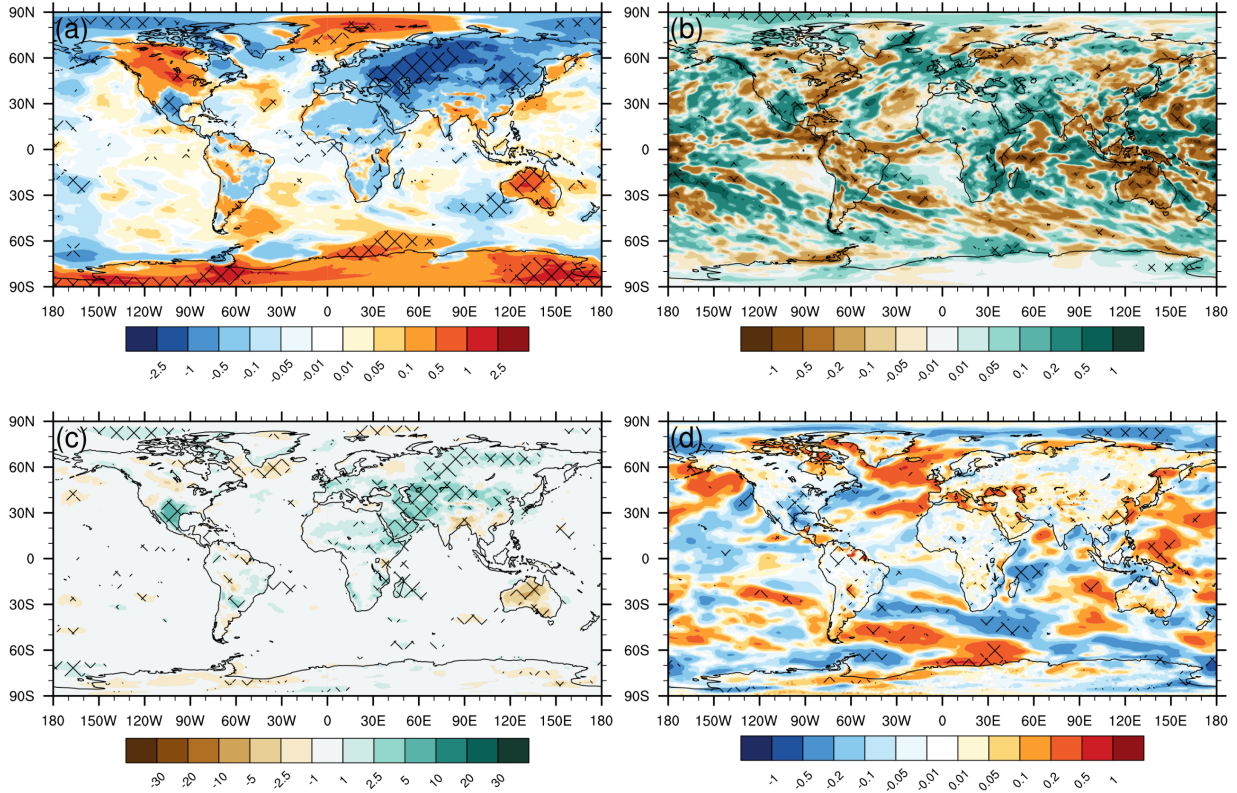
Figure 10: Fire induced changes in fire weather variables between the RCP4.5 future scenario and the present-day scenario ((CTRL2-CTRL1)-(SENS2B-SENS1B)). (a) fire induced changes in surface temperature (K); (b) fire induced changes in total precipitation rate (mm day⁻¹); (c) fire induced changes in surface relative humidity (%); (d) fire induced changes in surface wind speed (m s⁻¹). The hatchings denote the 0.05 significance level.

943
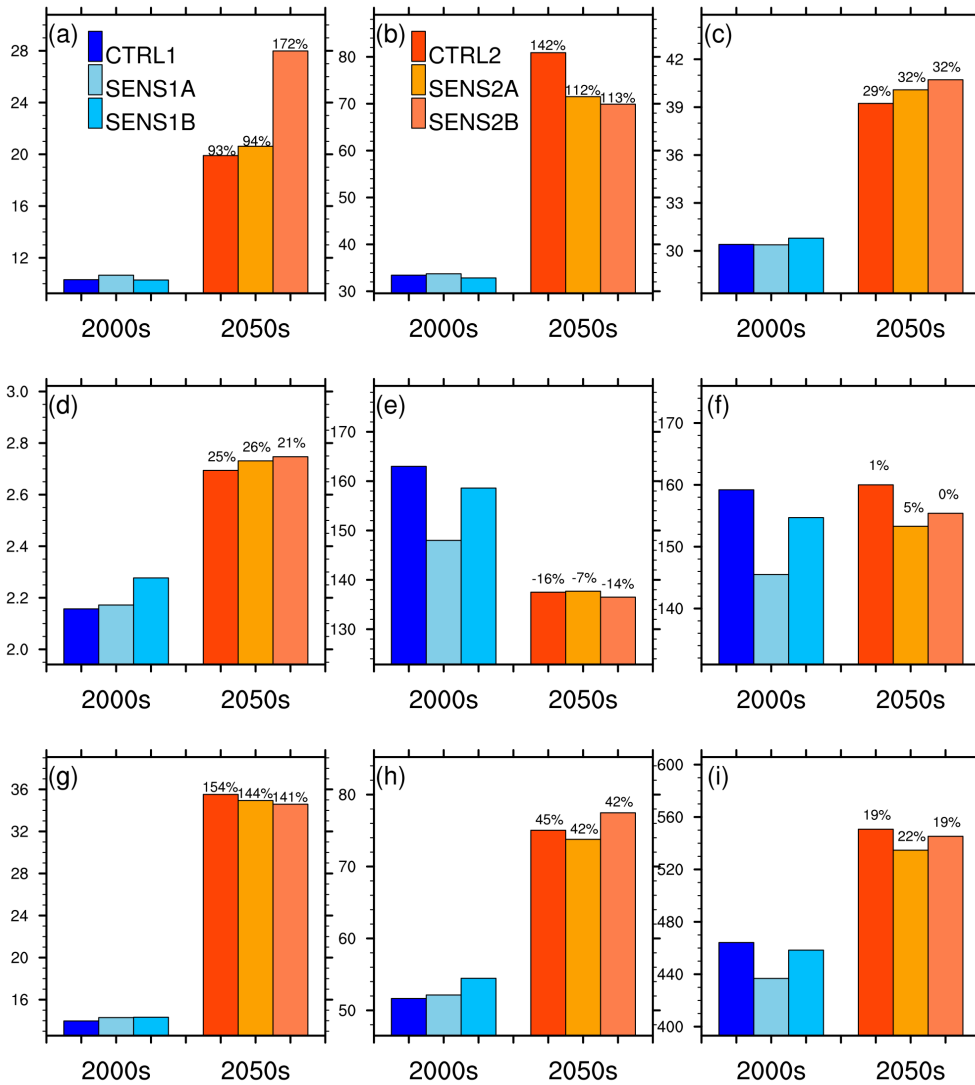
Figure 11: Comparison of annual burned area (Mha yr⁻¹) in each region among different time periods and sensitivity experiments. (a) North America; (b) South America; (c) Eurasia excluding Middle East and South Asia; (d) Middle East and North Africa; (e) Northern Hemisphere Africa; (f) Southern Hemisphere Africa; (g) South and Southeast Asia; (h) Oceania; (i) global total BA. The percentage numbers above projection columns are changes of burned area in the 2050s relative to their counterpart experiments in the 2000s. The spatial distributions of these regions are shown in Fig. S4 of the Supplement.

950
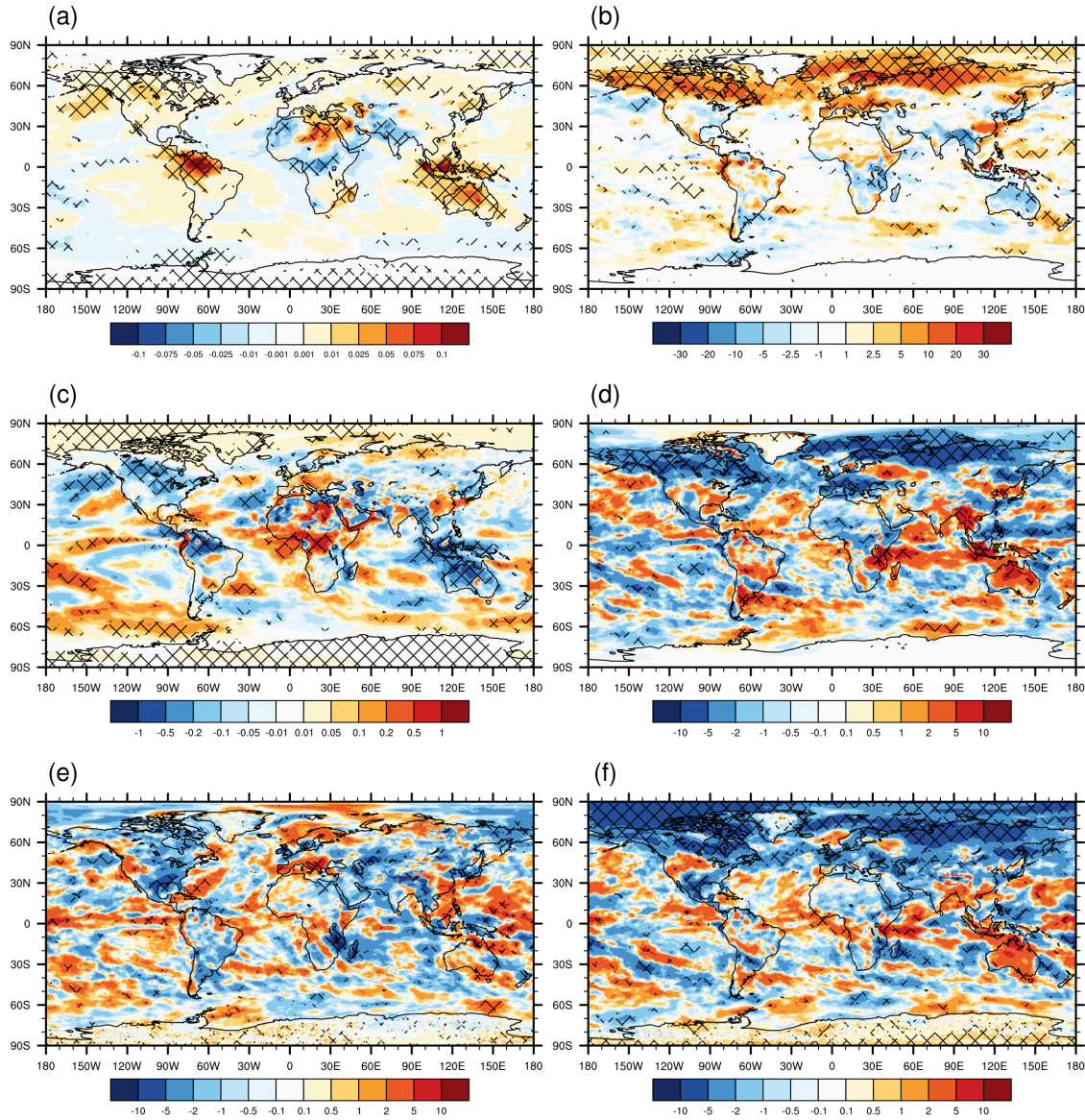
Figure 12: Changes in fire induced weather conditions and climate radiative forcing between the RCP4.5 future scenario and the present-day scenario. (a) changes in annual averaged column AOD at 550 nm (unitless, (CTRL2-SENS2A)-(CTRL1-SENS1A)); (b) changes in cloud liquid water path (g m⁻², (CTRL2-SENS2A)- (CTRL1-SENS1A)); (c) changes in RE_ari (W m⁻², (CTRL2-SENS2A)- (CTRL1-SENS1A)); (d) changes in RE_aci (W m⁻², (CTRL2-SENS2A)- (CTRL1-SENS1A)); (e) changes in RE_lcc (W m⁻², (SENS2A-SENS2B)- (SENS1A-SENS1B)); (f) changes in RE_fire (W m⁻², (CTRL2-SENS2B)- (CTRL1-SENS1B)). The hatchings denote the 0.05 significance level.

957
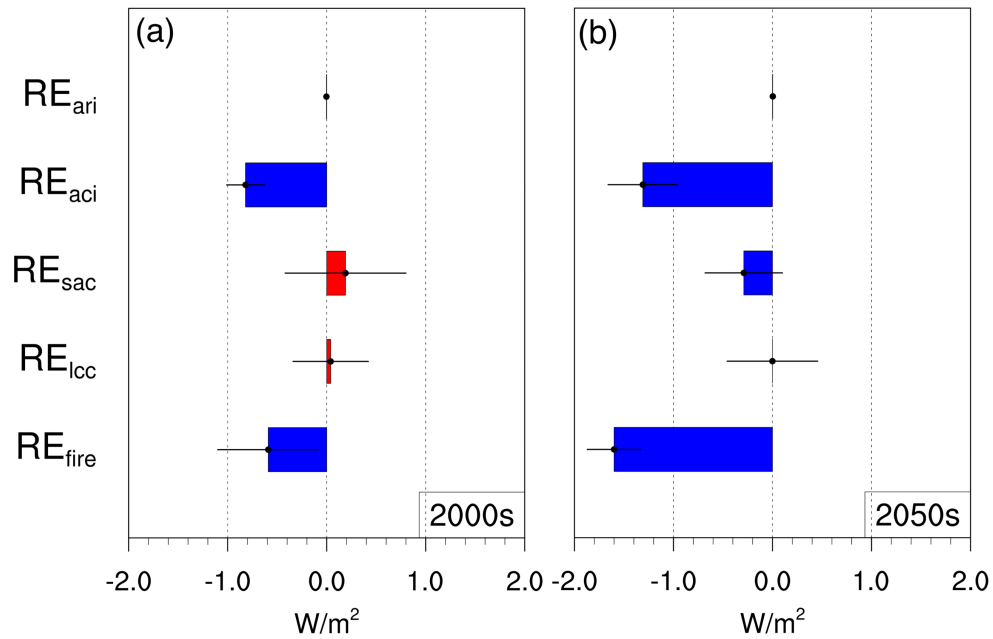
Figure 13: Comparison of CESM-RESFire simulated fire radiative effects (W m⁻²) in (a) the present-day scenario and (b)

958

the RCP4.5 future scenario. The error bars denote standard deviations of interannual variations during each 10-year

959

simulation period. RE$_{fire}$ denotes the net radiative effect of the four fire-related radiative effects investigated in this study

960

(RE$_{fire}$= RE$_{ari}$ + RE$_{aci}$ + RE$_{sac}$ + RE$_{lcc}$).

961

962

963 **Table 1: Fire sensitivity simulation experiments for the present-day and RCP4.5 future scenarios**

Scenario	Present-day (2000)			Future (RCP4.5)		
Name	CTRL1	SENS1A	SENS1B	CTRL2	SENS2A	SENS2B
Time	2001-2010	2001-2010	2001-2010	2051-2060	2051-2060	2051-2060
Atmosphere	CAM5	CAM5	CAM5	CAM5	CAM5	CAM5
Land	CLM4.5	CLM4.5	CLM4.5	CLM4.5	CLM4.5	CLM4.5
Ocean	Climatology	Climatology	Climatology	RCP4.5 data	RCP4.5 data	RCP4.5 data
Sea ice	Climatology	Climatology	Climatology	RCP4.5 data	RCP4.5 data	RCP4.5 data
Non-fire emissions	IPCC AR5 emission data	IPCC AR5 emission data	IPCC AR5 emission data	RCP4.5 data	RCP4.5 data	RCP4.5 data
Fire emissions	Online fire aerosols with plume rise	—	—	Online fire aerosols with plume rise	—	—
Land cover	Fire disturbance on present-day conditions	Fire disturbance on present-day conditions	Fixed present-day conditions in 2000	Fire disturbance on RCP4.5 conditions	Fire disturbance on RCP4.5 conditions	Fixed RCP4.5 conditions in 2050

964
965

966 **Table 2: Comparison of fire-related radiative effects in the present-day (CTRL1-SENS1A) and RCP4.5 future (CTRL2-**
967 **SENS2A) scenarios based on this work and previous studies**

Unit: W m^{-2}	This work		Jiang et al. (2016)	Ward et al. (2012)	
Time	2000s	2050s	2000s	2000s (CLM3/GFEDv2)	2100s (CCSM/ECHAM)
RE$_{ari}$	-0.003±0.013[a]	0.003±0.033	0.16±0.01	0.10/0.13	0.12/0.25
RE$_{aci}$	-0.82±0.19	-1.31±0.35	-0.70±0.05	-1.00/-1.64	-1.42/-1.74
RE$_{sac}$	0.19±0.61	-0.29±0.39	0.03±0.10	0.00/0.01	0.00/0.00
RE$_{aer}$	-0.64±0.48	-1.59±0.33	-0.55±0.07	-0.90/-1.50	-1.30/-1.49
RE$_{lcc}$	0.04±0.38	-0.006±0.457	—	-0.20/-0.11	-0.23/-0.29
RE$_{fire}$	-0.59±0.51	-1.60±0.27	-0.55±0.07	-0.55[b]/—	-0.83/-0.87[b]

968 [a]: the numbers after ± denote standard deviations of interannual variations;

969 [b]: the net radiative forcing includes other effects such as GHGs and climate-BGC feedbacks;

970

Table 3: Comparison of fire and carbon budget variables between CESM-RESFire simulations and previous studies and benchmarks

Variables	Time Period	This work		CLM-LL2013 (Li et al., 2014)	Benchmark	Sources
Models		RESFire-CRUNCEP	RESFire-CAM5c	CLM4.5-DATM		
Burned area (Mha yr^{-1})	1997-2004	508 ± 15	472 ± 14	322	510 ± 27	GFED4.1s (Giglio et al., 2013; Randerson et al., 2012)
Fire carbon emissions (Pg C yr^{-1})	1997-2004	2.3 ± 0.2	2.6 ± 0.1	2.1	2.2 ± 0.4	GFED4.1s (van der Werf et al., 2017)
NEE (Pg C yr^{-1})	1990s	-2.6 ± 0.6	-2.0 ± 1.3	-0.8	-1.1 ± 0.9 -2.0 ± 0.8	IPCC AR5 (Ciais et al., 2013) 10 models average (Piao et al., 2013)
GPP (Pg C yr^{-1})	2000-2004	142 ± 2	142 ± 1	130	133 ± 15	10 models average (Piao et al., 2013)
NPP (Pg C yr^{-1})	2000-2004	62 ± 1	63 ± 0.7	54	54	Zhao and Running (2010)

973

974

975 **Table 4: Comparison of carbon budget variables between the CRUNCEP data atmosphere driven fire simulations based**
976 **on CESM-RESFire and CLM-LL2013**

Variables	CESM-RESFire			CLM-LL2013 (Li et al., 2014)		
Unit: Pg C yr^{-1}	ΔFire	Fire on	Fire off	ΔFire	Fire on	Fire off
NEE	1.58	-2.67	-4.25	1.0	-0.1	-1.1
C_{fe}	2.08	2.08	0.0	1.9	1.9	0.0
-NEP+C_{lh}	-0.5	-4.75	-4.25	-0.9	-2.0	-1.1
NEP	0.5	4.8	4.3	0.8	3.0	2.3
NPP	0.4	61.7	61.3	-1.9	49.6	51.6
Rh	-0.1	56.9	57.0	-2.7	46.6	49.3
GPP	-0.1	142.3	142.4	-5.0	118.9	123.9
Ra	-0.5	80.6	81.1	-3.1	69.3	72.4
C_{lh}	0.0	0.05	0.05	-0.1	1.0	1.1

977
978

979 **Table 5: Comparison of carbon budget variables between CESM-RESFire sensitivity experiments and previous studies**

Variables	This work						Kloster et al. (2010)	
							Kloster et al. (2012)	
Time (scenario)	2000s (CTRL1)	2050s (CTRL2)	2000s (SENS1A)	2050s (SENS2A)	2000s (SENS1B)	2050s (SENS2B)	2000s	2050s
Burned area ($Mha\ yr^{-1}$)	464±19	551±16 (↑19%) [a]	437±17 (↓6%) [b]	535±19 (↓3%)	458±18 (↓1%)	545±18 (↓1%)	176-330	—
Fire carbon emissions ($Pg\ C\ yr^{-1}$)	2.5±0.1	5.0±0.3 (↑100%)	—	—	—	—	2.0-2.4	2.7/ 3.4
GPP ($Pg\ C\ yr^{-1}$)	141±1.2	146±1.1 (↑4%)	143±1.0 (↑1%)	149±1.3 (↑2%)	142±1.5 (↑1%)	150±1.3 (↑3%)	—	—
NEP ($Pg\ C\ yr^{-1}$)	1.4±0.04	1.5±0.04 (↑7%)	1.4±0.04 (→0%)	1.6±0.04 (↑7%)	1.4±0.02 (→0%)	1.6±0.05 (↑7%)	—	—
NEE ($Pg\ C\ yr^{-1}$)	1.2±0.03	1.6±0.05 (↑33%)	1.2±0.02 (→0%)	1.6±0.05 (→0%)	1.2±0.02 (→0%)	1.6±0.05 (→0%)	—	—

980 [a]: percentage numbers in the parentheses under CTRL2 denote relative changes comparing with the CTRL1
981 scenario.
982 [b]: percentage numbers in the parentheses under SENSx (x=1 or 2) denote relative changes comparing with the
983 corresponding CTRLx (x=1 or 2) scenarios.